

# Augmentation Invariant Manifold Learning

Shulei Wang

University of Illinois at Urbana-Champaign

(November 2, 2022)

## Abstract

Data augmentation is a widely used technique and an essential ingredient in the recent advance in self-supervised representation learning. By preserving the similarity between augmented data, the resulting data representation can improve various downstream analyses and achieve state-of-art performance in many applications. To demystify the role of data augmentation, we develop a statistical framework on a low-dimension product manifold to theoretically understand why the unlabeled augmented data can lead to useful data representation. Under this framework, we propose a new representation learning method called augmentation invariant manifold learning and develop the corresponding loss function, which can work with a deep neural network to learn data representations. Compared with existing methods, the new data representation simultaneously exploits the manifold’s geometric structure and invariant property of augmented data. Our theoretical investigation precisely characterizes how the data representation learned from augmented data can improve the  $k$ -nearest neighbor classifier in the downstream analysis, showing that a more complex data augmentation leads to more improvement in downstream analysis. Finally, numerical experiments on simulated and real datasets are presented to support the theoretical results in this paper.

---

\*Address for Correspondence: Department of Statistics, University of Illinois at Urbana-Champaign, 605 E. Springfield Ave., Champaign, IL 61820 (Email: shuleiw@illinois.edu).

# 1 Introduction

## 1.1 Data Augmentation in Representation Learning

Selecting low dimensional data features/representations is one of the most crucial components in various statistical and machine learning tasks, such as data visualization, clustering, and classifications. In these tasks, the performance of different statistical and machine learning methods usually relies largely on the choices of data representations (Guyon et al., 2008; Bengio et al., 2013). Although domain knowledge sometimes provides useful options to transform the raw data into features, it is still unclear which features can help the statistical methods achieve the best performance on a given data set. One promising solution to address this problem is to learn the explanatory data features/representations from the data itself. Numerous statistical and machine learning techniques are proposed to learn data-driven representations in the literature, including principal component analysis (PCA) (Jolliffe, 2002), manifold learning (Belkin and Niyogi, 2003; Coifman and Lafon, 2006), and autoencoders (Hinton and Zemel, 1993). See a comprehensive review in Bengio et al. (2013). The idea of learning data-driven representations has been widely used and successful in different applications, including genomics (Rhee et al., 2018; Chereda et al., 2019), natural language processing (Collobert et al., 2011; Devlin et al., 2019), biomedical imaging analysis (Chung and Weng, 2017; Kim et al., 2020), and computer vision (Caron et al., 2020; Jing and Tian, 2020).

In recent years, self-supervised representation learning, a popular and successful method, has been introduced to learn low-dimensional representations from unlabeled data (Hjelm et al., 2018; Chen et al., 2020b; He et al., 2020; Grill et al., 2020; Tian et al., 2020a; Chen and He, 2021; Zbontar et al., 2021). Unlike unsupervised techniques, the data representations are trained by the pseudo labels automatically generated from the unlabeled data set. Data augmentation is perhaps one of the most commonly-used ways to generate pseudo labels in self-supervised learning, such as image flipping, rotation, colorization, and cropping (Gidaris et al., 2018; Shorten and Khoshgoftaar, 2019). With augmented data, the self-supervised learning methods aim to preserve similarity between augmented data of the same sample.

The resulting data representations can improve existing statistical and machine learning methods to achieve state-of-art performance in many applications (Chen et al., 2020b; Grill et al., 2020; Tian et al., 2020a; Zbontar et al., 2021).

Despite the exciting empirical performance, there is still little understanding of how self-supervised representation learning and data augmentation works. Why can the data representations learned from the augmented data improve downstream analysis on labeled data? What structure information does self-supervised learning exploit from augmented data? Therefore, there is a clear need to develop a rigorous statistical framework to characterize the role of data augmentation and study how augmented data can lead to useful data representations for downstream analysis. In addition, most existing self-supervised representation learning methods mainly focus on capturing the information of augmented data alone, that is, the data representations of augmented data should be similar. A rich source of information often neglected by current self-supervised learning is the data’s low dimensional structure, which has been explicitly exploited by many classical representation learning methods, like principal component analysis and manifold learning. One may wonder if we could combine the information in augmented data and low dimensional structure to learn data representations better. We show this is feasible in this paper.

Since the introduction of self-supervised learning, recent works have tried to theoretically understand why the learned data representation from augmented data can help improve the downstream analysis (Arora et al., 2019; Tsai et al., 2020; Wei et al., 2020; Tian et al., 2020b; Tosh et al., 2021; Wen and Li, 2021; HaoChen et al., 2021; Wang, 2022; Wen and Li, 2022; Balestrierio and LeCun, 2022). Most of these theoretical works focus on the setting where the special conditional independence structure for the augmented data is assumed. For example, Arora et al. (2019) assumes the augmented data of the same sample is drawn from a conditional distribution of a discrete latent variable. Wang (2022) and Wen and Li (2021) assume the linear latent factor model for the augmented data. Beyond conditional independence structure, HaoChen et al. (2021) and Balestrierio and LeCun (2022) also study the contrastive methods from a spectral graph angle. Although the existing results can provide insights into how self-supervised representation learning methods work, some assumptions,

like the linear latent factor model, could be very restrictive in many applications, and there is a lack of understanding of the role of low dimensional structure in self-supervised learning and data augmentation. Motivated by these challenges, we introduce a new framework for self-supervised learning on a low-dimensional product manifold.

## 1.2 A Manifold Model for Data Augmentation

The high-dimensional data naturally arise in a wide range of applications, including computer vision and genetics. Despite the high dimensionality of conventional representation, there is strong empirical evidence that the data is highly concentrated in a low-dimensional manifold in these applications. For example, a recent study in (Pope et al., 2021) suggests that the intrinsic dimensions of images in dataset ImageNet and CIFAR-10 are less than 45 and 30. Motivated by this observation, we assume the observed data (before and after data augmentation) lie in a  $d$ -dimensional manifold  $\mathcal{M} \subset \mathbb{R}^D$  in this paper.

Suppose we apply the data augmentation technique to a data set of  $m$  samples and obtain a multi-view data set  $(X_{i,1}, \dots, X_{i,n})$ ,  $i = 1, \dots, m$ , where  $n$  different augmented data of each sample are observed. The augmented data are usually obtained by some transformation, such as flipping, rotation, colorization, and scaling (Shorten and Khoshgoftaar, 2019). To model the transformation, we assume the manifold  $\mathcal{M}$  is an isometric embedding of a product manifold

$$\mathcal{M} = T(\mathcal{N}_s \times \mathcal{N}_v), \quad (1)$$

where  $T$  is an isometry and  $\mathcal{N}_s, \mathcal{N}_v$  are two no-boundary manifolds with dimensions  $d_s$  and  $d_v$  such that  $d = d_s + d_v$ . Here,  $\mathcal{N}_s$  represents the structure of interest and  $\mathcal{N}_v$  corresponds to irrelevant nuisance structures resulting from data augmentation. Given the product manifold assumption, we consider the following way to generate the multi-view augmented data

$$\phi_1, \dots, \phi_m \stackrel{i.i.d.}{\sim} f_s(\phi) \quad \text{and} \quad \psi_{i,1}, \dots, \psi_{i,n} \stackrel{i.i.d.}{\sim} f_v(\psi|\phi_i),$$

where  $f_s(\phi)$  is some conditional probability density function defined on  $\mathcal{N}_s$  and  $f_v(\psi|\phi_i)$  is some probability density function defined on  $\mathcal{N}_v$ . Our observed augmented data is  $X_{i,j} = T(\phi_i, \psi_{i,j})$  for  $i = 1, \dots, m$  and  $j = 1, \dots, n$ . Similar models are also considered in Berry and

Harlim (2018); Lederman and Talmon (2018); Talmon and Wu (2019); Salhov et al. (2020); Lindenbaum et al. (2020), but their sampling processes are different from our model. This model indicates that each sample’s augmented data lies in a manifold  $\mathcal{M}$ ’s fiber

$$X_{i,1}, \dots, X_{i,n} \in \mathcal{M}(\phi_i),$$

where  $\mathcal{M}(\phi) = \{x \in \mathcal{M} : x = T(\phi, \psi), \psi \in \mathcal{N}_v\}$ . The elements within the same fiber are equivalent up to some data augmentation transformation.

Given the data augmentation model, what are the desired data representations? Here, the data representation is defined as a map  $\Theta : \mathcal{M} \rightarrow \mathbb{R}^N$ .

- **Augmentation invariant** Similar to other self-supervised learning methods, the desired data representation should preserve similarity between augmented data of the same sample since it is usually believed that data augmentation only perturbs irrelevant information (Chan et al., 2021). Putting mathematically, the map  $\Theta$  is invariant to data augmentation

$$\Theta(x) = \Theta(y), \quad \text{if } x, y \in \mathcal{M}(\phi).$$

- **Local similarity** As the data lie on a low-dimensional manifold, the desired data representations should be able to capture the intrinsic geometric structure and preserve the local information. More concretely, the map  $\Theta$  should map similar samples to similar data representations, that is,

$$\phi_x \approx \phi_y \quad \Leftrightarrow \quad \Theta(x) \approx \Theta(y), \quad x \in \mathcal{M}(\phi_x), y \in \mathcal{M}(\phi_y).$$

These two good properties make one wonder if such an ideal map exists and, if so, how we should find it based on the augmented data  $(X_{i,1}, \dots, X_{i,n}), i = 1, \dots, m$ .

### 1.3 A Peek at Augmentation Invariant Manifold Learning

This paper’s primary goal is to introduce a new representation learning framework for the augmented data, called augmentation invariant manifold learning. The new framework is

simple as it shares a similar procedure with classical manifold learning methods, Laplacian eigenmaps (Belkin and Niyogi, 2003), and diffusion maps (Coifman and Lafon, 2006). The main difference from these two classical manifold learning methods is that augmentation invariant manifold learning integrates the kernels between any pair of augmented data to evaluate the similarity between two samples

$$W_{i_1, i_2} = \frac{1}{n^2} \sum_{j_1, j_2=1}^n \exp\left(-\frac{\|X_{i_1, j_1} - X_{i_2, j_2}\|^2}{t}\right),$$

where  $t > 0$ . Our investigation shows that, with this simple modification, augmentation invariant manifold learning can recover the eigenvalues and eigenfunctions of the Laplace-Beltrami operator on  $\mathcal{N}_s$  instead of  $\mathcal{M}$ . Therefore, the data representation learned from augmentation invariant manifold learning 1) is invariant to data augmentation and 2) can capture the intrinsic geometric structures of the underlying manifold.

To better illustrate the idea, we consider a simple example where  $\mathcal{N}_s = \mathcal{N}_v = S^1$  where  $S^1$  is a circle, and  $\mathcal{M} = S^1 \times S^1$  is a torus in 3 dimensional space  $x = (x_1, x_2, x_3)$  such that  $x_1 = (10 + 5 \cos \phi) \cos \psi$ ,  $x_2 = (10 + 5 \cos \phi) \sin \psi$ , and  $x_3 = 5 \sin \phi$ . We choose  $m = 400$  and  $n = 3$  in the augmented data. If we only consider the first two eigenvectors in augmentation invariant Laplacian eigenmaps as our data representation, Figure 1 shows the plots of representations colored by the value of  $\phi$  and  $\psi$ . The data representation from augmentation invariant Laplacian eigenmaps can capture the information on  $\mathcal{N}_s$  very well and is invariant to different  $\psi$ 's choices.

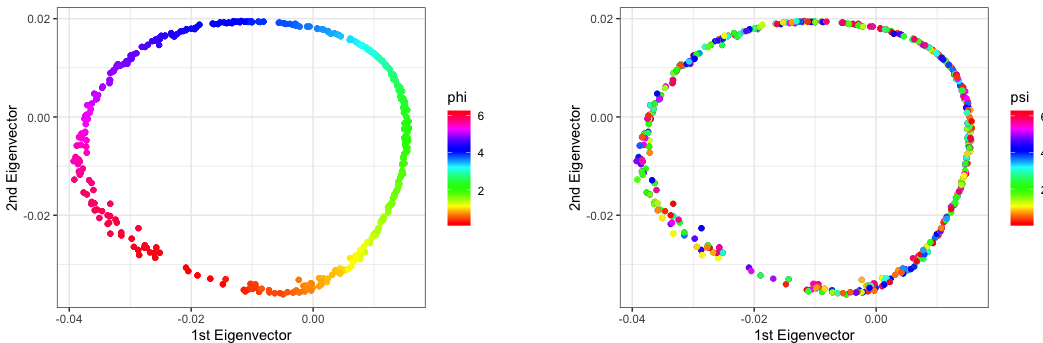


Figure 1: Plots of new data representation colored by the value of  $\phi$  (left) and  $\psi$  (right).

The new data representation is invariant to data augmentation, but can it help improve downstream analyses? Our analysis shows that the new data representation can lead to more powerful  $k$ -nearest neighbor ( $k$ -NN) classifier if we further assume  $\gamma(x) = \gamma(y)$  for any  $x, y \in \mathcal{M}(\phi)$ , where  $\gamma(x) = \mathbb{P}(Y = 1|X = x)$  is the regression function. Specifically, when we compare the original  $X$  and new data representation  $\Theta(X)$ , the excess risk of misclassification error of  $k$ -NN can be improved by

$$s^{-\alpha(1+\beta)/(2\alpha+d)} \quad \Rightarrow \quad s^{-\alpha(1+\beta)/(2\alpha+d_s)},$$

where  $s$  is the sample size in downstream analysis,  $\alpha$  and  $\beta$  are the smoothness of the regression function and parameter for the Tsybakov margin condition, and  $d$  and  $d_s$  are the dimensions of  $\mathcal{M}$  and  $\mathcal{N}_s$ . The intuitive explanation behind this improvement is that points in the neighborhood defined by  $\Theta(X)$  have more similar values in  $\phi$  than in the neighborhood defined by  $X$ . In Figure 2, we illustrate this intuition by comparing the neighborhood defined by different representations in previous torus example. The results here also suggest that a more complex data augmentation (larger  $d_v$  and thus smaller  $d_s$ ) can lead to more improvement in the downstream analysis, which is consistent with the empirical observation in Chen et al. (2020b).

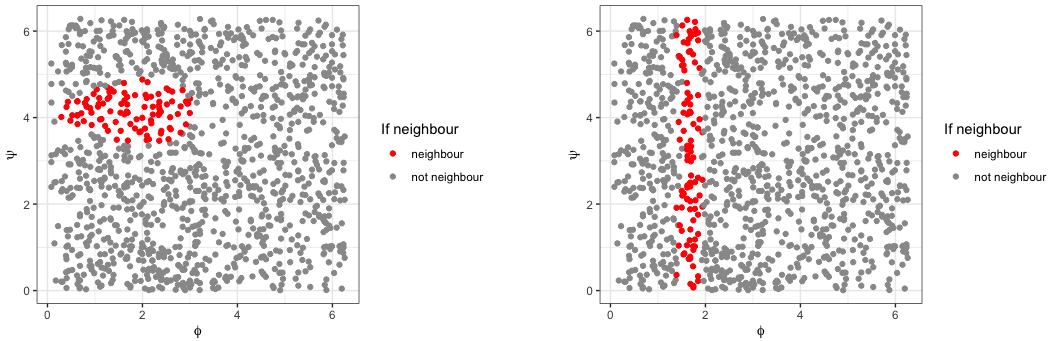


Figure 2: Neighborhood defined by  $X$  (left) and new data representation  $\Theta(X)$  (right).

The augmentation invariant manifold learning can also lead to a new loss function if we parameterize the data representation maps as  $\Theta_\beta$  where  $\beta \in \mathcal{B}$ , e.g., a deep neural network

encoder. Specifically, the augmentation invariant data representation can be obtained by minimizing the following objective function, including both unsupervised and self-supervised signal,

$$\min_{\beta \in \mathcal{B}} \underbrace{\sum_{i=1}^m W_{i,i^-} \|\Theta_{\beta}(X_i) - \Theta_{\beta}(X_{i^-})\|^2}_{\text{unsupervised signal}} + \lambda_1 \underbrace{\sum_{i=1}^m \|\Theta_{\beta}(X_i) - \Theta_{\beta}(X_{i^+})\|^2}_{\text{self-supervised signal}} + \underbrace{\lambda_2 \mathcal{R}(\Theta_{\beta})}_{\text{regularization}},$$

where  $(X_i, X_{i^+})$  is a pair of augmented data of the same sample,  $(X_i, X_{i^-})$  is a pair of data from different samples,  $W_{i,i^-}$  is the weight between  $X_i$  and  $X_{i^-}$ ,  $\mathcal{R}(\Theta_{\beta})$  is the regularization term, and  $\lambda_1, \lambda_2$  are tuning parameters. Unlike existing self-supervised representation learning methods, the new loss function keeps the local similarity between negative data pairs and adds a regularization term to avoid dimensional collapse. Since modern optimization techniques can be applied, the new loss function can be seen as a generalizable and computational efficient version of augmentation invariant manifold learning.

## 2 Augmentation Invariant Manifold Learning

### 2.1 Classical Manifold Learning

Several different nonlinear methods are proposed in the literature to extract features from the data lying on a low-dimensional manifold, including Isomap (Tenenbaum et al., 2000), locally linear embedding (LLE) (Roweis and Saul, 2000), maximum variance unfolding (Weinberger and Saul, 2006), Hessian maps (Donoho and Grimes, 2003), Laplacian eigenmaps (Belkin and Niyogi, 2003), local tangent space alignment (Zhang and Zha, 2004), diffusion maps (Coifman and Lafon, 2006), and vector diffusion map (Singer and Wu, 2012). Most manifold learning algorithms explore the locally linear structure of the underlying manifold. In particular, the spectral graph-based method, such as Laplacian eigenmaps and diffusion maps, is one of the most popular strategies, which constructs a graph by connecting close points and then using the eigenvectors of graph Laplacian as data representation.

Suppose  $\theta : \mathcal{M} \rightarrow \mathbb{R}$  is a twice differentiable map that aims to preserve the local information. As suggested by Belkin and Niyogi (2003), if we aim to find a map that can preserve



the local similarity of nearby points, we can consider the following optimization problem for Dirichlet energy

$$\min_{\|\theta\|_{L^2(\mathcal{M})}=1} \int_{\mathcal{M}} \|\nabla\theta(x)\|^2 dx,$$

where  $dx$  is with respect to the Riemannian volume form of  $\mathcal{M}$ . By Stokes' theorem, this is equivalent to the following optimization problem

$$\min_{\|\theta\|_{L^2(\mathcal{M})}=1} \int_{\mathcal{M}} \mathcal{L}(\theta)\theta(x)dx,$$

where  $\mathcal{L}$  is the Laplace-Beltrami operator on  $\mathcal{M}$ . Therefore, the solution for the optimization problem for Dirichlet energy is the eigenfunctions of the Laplace-Beltrami operator.

In practice, we only observe a collection of points  $X_1, \dots, X_m$  randomly drawn from the manifold  $\mathcal{M}$  instead of knowing the manifold  $\mathcal{M}$  exactly. We can consider a discrete version of Dirichlet energy

$$\min_{\theta_1, \dots, \theta_m: \sum_i \theta_i^2 = 1} \frac{1}{2} \sum_{i_1, i_2 = 1}^m W_{i_1, i_2} (\theta_{i_1} - \theta_{i_2})^2,$$

where  $W_{i_1, i_2}$  is the weight of the edge connecting  $X_{i_1}$  and  $X_{i_2}$  and  $\theta_i = \theta(X_i)$ . There are several different ways to choose the weights  $W_{i_1, i_2}$ . For example, Laplacian eigenmaps adopts the following weight

$$W_{i_1, i_2} = \frac{h_t(\|X_{i_1} - X_{i_2}\|)}{\sqrt{\sum_{i_3=1}^m h_t(\|X_{i_1} - X_{i_3}\|)} \sqrt{\sum_{i_3=1}^m h_t(\|X_{i_2} - X_{i_3}\|)}}$$

where  $h_t(z) = \exp(z^2/t)$ . Given the weight matrix  $W$ , we introduce the graph Laplacian  $L = D - W$ , where  $D$  is the degree matrix of  $W$ , that is,  $D$  is a diagonal matrix such that  $D_{i,i} = \sum_{i'=1}^m W_{i,i'}$ . Since the graph Laplacian  $L$  converges to the Laplace-Beltrami operator  $\mathcal{L}$  (Belkin and Niyogi, 2008), it is sufficient to find the eigenvectors of  $L$  to estimate the eigenfunctions of Laplace-Beltrami operator  $\mathcal{L}$ . The data representation resulting from  $L$ 's eigenvectors can capture the intrinsic geometric structures of  $\mathcal{M}$  but is not augmentation invariant.

## 2.2 Augmentation Invariant Manifold Learning

Besides manifold assumption, we have extra information on which two data points are equivalent in the augmented data. How shall we incorporate such information to find an aug-

mentation invariant data representation? We still consider the optimization problem for Dirichlet energy, but need to add a constraint for augmented data

$$\min_{\|\theta\|_{L^2(\mathcal{M})}=1} \int_{\mathcal{M}} \|\nabla\theta(x)\|^2 dx, \quad \text{s.t. } \theta(x) = \theta(y), \quad \text{if } x, y \in \mathcal{M}(\phi). \quad (2)$$

The constraint requires that  $\theta$  has the same value on  $\mathcal{M}(\phi)$  for each  $\phi$  so that we can write any  $\theta(x)$  satisfying this constraint as  $\theta(x) = \tilde{\theta}(\phi)$  for some function  $\tilde{\theta}$  defined on  $\mathcal{N}_s$ . Therefore, the above optimization problem can be reformulated as

$$\min_{\|\tilde{\theta}\|_{L^2(\mathcal{N}_s)}=1} \int_{\mathcal{N}_s} \|\nabla\tilde{\theta}(\phi)\|^2 d\phi.$$

By Stokes' theorem again, the solution in the above optimization problem is the eigenfunctions of Laplace Beltrami operator  $\mathcal{L}_{\mathcal{N}_s}$  on  $\mathcal{N}_s$ , which are augmentation invariant.

To estimate these eigenfunctions from the observed data, we can still consider the similar discrete version of Dirichlet energy in (2)

$$\min_{\sum_{i,j} \theta_{i,j}^2=1} \frac{1}{2} \sum_{i_1, i_2=1}^m \sum_{j_1, j_2=1}^n W_{i_1, j_1, i_2, j_2} (\theta_{i_1, j_1} - \theta_{i_2, j_2})^2, \quad \text{s.t. } \theta_{i,1} = \dots = \theta_{i,n}, i = 1, \dots, m, \quad (3)$$

where  $W_{i_1, j_1, i_2, j_2}$  is the weight of the edge connecting  $X_{i_1, j_1}$  and  $X_{i_2, j_2}$  and  $\theta_{i,j} = \theta(X_{i,j})$ . If we write  $\theta_i = \theta_{i,1} = \dots = \theta_{i,n}$ , the above optimization problem can be reformulated as the following equivalent problem

$$\min_{\theta_1, \dots, \theta_m: \sum_i \theta_i^2=1} \frac{1}{2} \sum_{i_1, i_2=1}^m W_{i_1, i_2} (\theta_{i_1} - \theta_{i_2})^2, \quad \text{where } W_{i_1, i_2} = \sum_{j_1, j_2=1}^n W_{i_1, j_1, i_2, j_2}.$$

Compared with the classical spectral graph-based method, the main difference is that the weights between all possible augmented data of two samples are combined into a single weight. Integrating several kernels/weights is also used in solving sensor fusion problems (Gustafsson, 2010; Lahat et al., 2015), which aims to extract common information from several different sensors (Lederman and Talmon, 2018; Talmon and Wu, 2019; Lindenbaum et al., 2020). In the sensor fusion problem, the data from different sensors are usually from different spaces and thus not comparable, so only the kernel for the data from the same sensor(view) is considered. Unlike methods designed for sensor fusion problems, we evaluate the weights on all augmented data pairs of two samples because the augmented data lie on the same manifold  $\mathcal{M}$ .

---

**Algorithm 1** Augmentation Invariant Laplacian Eigenmaps

---

**Input:** A set of augmented data:  $(X_{i,1}, \dots, X_{i,n})$ ,  $i = 1, \dots, m$ .

Step 1: Calculate the weights between samples

$$W_{i_1, i_2} = \frac{1}{n^2} \sum_{j_1, j_2=1}^n \exp\left(-\frac{\|X_{i_1, j_1} - X_{i_2, j_2}\|^2}{t}\right), \quad i_1, i_2 = 1, \dots, m.$$

Step 2: Find the Laplacian matrix  $L = D - W$  where  $D$  is a diagonal degree matrix of  $W$ , i.e.,  $D_{i,i} = \sum_j W_{i,j}$ .

Step 3: Find the first  $N$  eigenvectors  $\vec{\eta}_1, \dots, \vec{\eta}_N$  for the generalized eigenvector problem

$$L\vec{\eta} = \lambda D\vec{\eta}.$$

**Output:** The representation for each sample:  $(X_{i,1}, \dots, X_{i,n}) \rightarrow (\eta_{1,i}, \dots, \eta_{N,i})$

---

To find the data representation, we can apply the idea of integrating weights to most spectral graph-based methods, such as Laplacian eigenmaps and diffusion maps. For example, Algorithm 1 is the augmentation invariant Laplacian eigenmaps method, combining the weights on all augmented data pairs of two samples. Algorithm 2 in Appendix A is the augmentation invariant version of diffusion maps. In the next section, we will show that the data representation found by these algorithms is indeed augmentation invariant.

## 2.3 Convergence Analysis

In this section, we show that the empirical data representation in Algorithm 1 converges to the eigenfunctions of Laplace Beltrami operator  $\mathcal{L}_\phi$  on  $\mathcal{N}_s$ . To study the theoretical properties, we must define the point cloud operators in Algorithm 1 carefully. Specifically, given  $\phi \in \mathcal{N}_s$ , we write

$$W_n(\phi_i, \phi_{i'}) = \frac{1}{n^2} \sum_{j, j'=1}^n \exp\left(-\frac{\|X_{i,j} - X_{i',j'}\|^2}{t}\right)$$

and

$$W_n(\phi_i, \phi) = \frac{1}{n} \sum_{j=1}^n \int_{\mathcal{M}(\phi)} \exp\left(-\frac{\|X_{i,j} - x\|^2}{t}\right) f_v(x|\phi) dx.$$

The point cloud operator in Algorithm 1 is defined as

$$L_{m,n}^t g(\phi) = \frac{1}{m} \sum_{i=1}^m \frac{1}{t} \frac{W_n(\phi_i, \phi)}{\sqrt{D_{m,n}^t(\phi)} \sqrt{D_{m,n}^t(\phi_i)}} (g(\phi) - g(\phi_i)),$$

where  $g(\phi)$  is a function defined on  $\mathcal{N}_s$ , and  $D_{m,n}^t(\phi)$  and  $D_{m,n}^t(\phi_i)$  are

$$D_{m,n}^t(\phi) = \frac{1}{m} \sum_{i=1}^m W_n(\phi_i, \phi) \quad \text{and} \quad D_{m,n}^t(\phi_i) = \frac{1}{m} \sum_{i'=1}^m W_n(\phi_i, \phi_{i'}).$$

The following theorem shows that the point cloud operator converges to the weighted Laplace Beltrami operator on  $\mathcal{N}_s$  so that the data representation in Algorithm 1 are eigenvectors of the Laplace Beltrami operator.

**Theorem 1.** *Suppose that  $f_v(\psi|\phi)$  is uniform distribution on  $\mathcal{M}(\phi)$  for any  $\phi$ , there exists a constant  $\kappa$  such that  $1/\kappa < f_s(\phi) < \kappa$ , and  $f_s(\phi)$  is twice differentiable. If we choose  $t = m^{-1/(d+4)}$ , then*

$$\lim_{m \rightarrow \infty} L_{m,n}^t g(\phi) = \frac{1}{2} \mathcal{L}_{\mathcal{N}_s, f_s} g(\phi),$$

where  $\mathcal{L}_{\mathcal{N}_s, f_s}$  is weighted Laplace Beltrami operator  $\mathcal{L}_{\mathcal{N}_s, f_s} g(\phi) = f_s^{-1}(\phi) \operatorname{div}(f_s(\phi) \nabla_{\mathcal{N}_s} g(\phi))$  and the limit is taken in probability. In particular, if  $f_s$  is uniform distribution on  $\mathcal{N}_s$ , we have

$$\lim_{m \rightarrow \infty} L_{m,n}^t g(\phi) = \frac{1}{2} \mathcal{L}_{\mathcal{N}_s} g(\phi),$$

where  $\mathcal{L}_{\mathcal{N}_s}$  is Laplace Beltrami operator on  $\mathcal{N}_s$ .

This theorem suggests that the operator in Algorithm 1 converges to the weighted Laplace Beltrami operator on  $\mathcal{N}_s$ . Instead of  $\mathcal{M}$ , the eigenvectors are defined on  $\mathcal{N}_s$  so that they are augmentation invariant. The intuition behind the results is that the weight in Algorithm 1 uses a randomized kernel defined on  $\mathcal{N}_s$ , and the expectation of the randomized kernel is

$$\mathbb{E}(W_{i_1, i_2}) = \frac{1}{\operatorname{Vol}^2 \mathcal{N}_v} \int_{\mathcal{M}(\phi_1)} \int_{\mathcal{M}(\phi_2)} \exp\left(\frac{\|x - y\|^2}{t}\right) dx dy,$$

while the classical manifold learning uses a deterministic kernel to evaluate weight. We can also show similar results for augmentation invariant diffusion maps in Algorithm 2 (see Theorem 4).

### 3 Benefits for Downstream Analysis

The last section shows that Algorithms 1 and 2 can find augmentation invariant representation when integrating information between augmented data. One may wonder whether the new data representation can help improve downstream analysis. If yes, to what extent can the new data representation improve the downstream analysis? To answer these questions, we study how the new data representation help improve one of the most popular classification methods: the  $k$ -nearest neighbor ( $k$ NN) classifier (Fix, 1985; Altman, 1992; Biau and Devroye, 2015).

To be specific, suppose we observe a collection of data  $(X_1, Y_1), \dots, (X_s, Y_s)$  in the downstream task such that  $X_1, \dots, X_s \in \mathcal{M}$  and  $Y_1, \dots, Y_s \in \{-1, 1\}$ . The goal is to build a classifier  $h : \mathcal{M} \rightarrow \{-1, 1\}$  to predict the label  $Y$  for any given input  $X$ . The high-level idea in  $k$ NN is that the majority vote of  $k$ -nearest neighbor is the predicted label. Specifically, the  $k$ NN classifier is defined as the following:

$$\hat{h}_X(x) = \begin{cases} 1, & \sum_{i=1}^k \mathbf{I}(Y_{(i)} = 1) > k/2 \\ -1, & \text{otherwise} \end{cases},$$

where  $(X_{(1)}, Y_{(1)}), \dots, (X_{(s)}, Y_{(s)})$  is a permutation of  $(X_1, Y_1), \dots, (X_s, Y_s)$  such that  $\|X_{(1)} - x\| \leq \dots \leq \|X_{(s)} - x\|$ . For simplicity, we always use Euclidean distance  $\|\cdot\|$  here. We can define the  $k$ NN classifier  $\hat{h}_{\Theta(X)}(x)$  similarly when we adopt data representation  $\Theta(X)$ . Unlike  $\hat{h}_X(x)$ , the  $k$  nearest neighbors in  $\hat{h}_{\Theta(X)}(x)$  is defined by a permutation of  $\Theta(X_1), \dots, \Theta(X_s)$  rather than the original data, that is,  $\|\Theta(X_{(1)}) - \Theta(x)\| \leq \dots \leq \|\Theta(X_{(s)}) - \Theta(x)\|$ . The goal of this section is to compare the performance of  $\hat{h}_{\Theta(X)}(x)$  and  $\hat{h}_X(x)$ .

#### 3.1 Infinite Samples

To study the effect of new data representation, we consider the ideal case that infinite samples are observed in the augmentation invariant manifold learning stage, that is,  $m = \infty$ . In other words, we know exactly the Laplace Beltrami operator on  $\mathcal{N}_s$  and its eigenfunctions. Specifically, we consider two types of data representations in this section

$$\Theta_1(x) = (\eta_1(\phi), \dots, \eta_N(\phi)) \quad \text{and} \quad \Theta_2(x) = (e^{-l\lambda_1}\eta_1(\phi), \dots, e^{-l\lambda_N}\eta_N(\phi)),$$

where  $x = T(\phi, \psi)$ ,  $\eta_1(\phi), \dots, \eta_N(\phi)$  are the first  $N$  eigenfunctions of  $\mathcal{L}_{\mathcal{N}_s}$ , and  $0 = \lambda_0 < \lambda_1 \leq \dots \leq \lambda_N$  are corresponding eigenvalues.  $\Theta_1(x)$  and  $\Theta_2(x)$  can be recovered by Algorithms 1 and 2, respectively. To compare  $\hat{h}_X(x)$ ,  $\hat{h}_{\Theta_1(X)}(x)$ , and  $\hat{h}_{\Theta_2(X)}(x)$ , we consider the excess risk of misclassification error as our performance measure

$$r(\hat{h}) = \mathbb{E} \left( \mathbb{P}(Y \neq \hat{h}(X)) \right) - \mathbb{P}(Y \neq h^*(X)),$$

where  $\hat{h}$  is a classifier estimated from the data and  $h^*$  is the optimal Bayes classification rule. To characterize the theoretical properties of  $k$ NN, we consider the following assumptions:

**Assumption 1.** *It holds that*

(a) *Let  $\gamma(x) = \mathbb{P}(Y = 1|X = x)$  be the regression function. We assume*

$$\gamma(x) = \gamma(y), \quad \text{if } x, y \in \mathcal{M}(\phi).$$

*In other words, there exists a function  $\tilde{\gamma}$  on  $\mathcal{N}_s$  such that  $\gamma(x) = \gamma(T(\phi, \psi)) = \tilde{\gamma}(\phi)$ ;*

(b)  *$\tilde{\gamma}(\phi)$  is  $\alpha$ -Hölder continuous, i.e.,  $|\tilde{\gamma}(\phi) - \tilde{\gamma}(\phi')| \leq Ld_{\mathcal{N}_s}(\phi, \phi')^\alpha$ , where  $\phi, \phi' \in \mathcal{N}_s$ ;*

(c) *The distribution of  $X$  satisfies  $\beta$ -marginal assumption on  $\mathcal{M}$ , i.e.,  $\mathbb{P}(0 < |\gamma(X) - 1/2| \leq t) \leq C_0 t^\beta$  for some constant  $C_0$ ;*

(d)  *$\mathcal{M}$  is a compact manifold. If we write the probability density function of  $X$  as  $f_\mu(x)$ , we assume  $1/\kappa \leq f_\mu(x) \leq \kappa$  for some  $\kappa > 1$ .*

(e) *The volume of manifold  $\mathcal{M}$  is upper bounded by  $V > 0$ , the Ricci curvature on  $\mathcal{M}$  is bounded below by  $\zeta > 0$ , and the injectivity radius on  $\mathcal{M}$  is bounded below by  $\iota > 0$ .*

The first assumption is the key assumption for data augmentation. It is usually believed that the data augmentation cannot change the label of the data (Chen et al., 2020a), so we can assume  $\gamma(x)$  has the same value on  $\mathcal{M}(\phi)$ . The next three assumptions are standard conditions used in the theoretical investigation of  $k$ NN (Audibert and Tsybakov, 2007; Samworth, 2012; Wang, 2022), but we extend them to the manifold setting here. The last assumption is used to characterize how many eigenfunctions are needed to represent the manifold (Bates, 2014; Portegies, 2016). With these assumptions, the following theorem shows the convergence rate of excess risk in  $\hat{h}_X(x)$ ,  $\hat{h}_{\Theta_1(X)}(x)$ , and  $\hat{h}_{\Theta_2(X)}(x)$ .

**Theorem 2.** *Suppose the Assumption 1 holds. There exists constants  $l_0$  and  $N_0$  (relying on  $d_s$ ,  $V$ ,  $\kappa$ , and  $\iota$ ) such that if we choose  $N = N_0$ ,  $l = l_0$  in  $\Theta_1(X)$  and  $\Theta_2(X)$ , and  $k \asymp s^{2\alpha/(2\alpha+d_s)}$ , then*

$$r(\hat{h}_{\Theta_1(X)}) \lesssim (e^{-d_s l_0 \lambda_{N_0} s})^{-\frac{\alpha(1+\beta)}{2\alpha+d_s}} \quad \text{and} \quad r(\hat{h}_{\Theta_2(X)}) \lesssim s^{-\frac{\alpha(1+\beta)}{2\alpha+d_s}}.$$

*If we choose  $k \asymp s^{2\alpha/(2\alpha+d)}$ , then we have*

$$r(\hat{h}_X) \lesssim s^{-\frac{\alpha(1+\beta)}{2\alpha+d}}.$$

*Here  $d$  and  $d_s$  are the dimensions of  $\mathcal{M}$  and  $\mathcal{N}_s$ .*

Here, we write  $a \lesssim b$  for two sequences  $a$  and  $b$  if there exists a constant  $C$  such that  $a \leq Cb$ . Theorem 2 provides the upper bound for the convergence rate of  $\hat{h}_X(x)$ ,  $\hat{h}_{\Theta_1(X)}(x)$ , and  $\hat{h}_{\Theta_2(X)}(x)$ . These upper bounds are sharp since they match the lower bounds for the flat manifold, i.e., subspace (Wang, 2022). A comparison between these convergence rates suggests the new data representation can improve the performance of  $k$ NN, and the data representation in the diffusion map,  $\Theta_2(x)$ , is a better choice than  $\Theta_1(x)$ .

## 3.2 Finite Samples

In the last section, we show that new data representation can improve  $k$ NN when we know  $\Theta_1(x)$  and  $\Theta_2(x)$  in advance. However, in practice, we still need to estimate the data representation from the unlabeled augmented data. One may naturally wonder if the data representation estimated by Algorithms 1 or 2 can still help improve  $k$ NN similarly. In this section, we show that this is possible when the sample size of the unlabeled augmented data is sufficiently large. In particular, we shall focus on augmentation invariant diffusion maps with parameter  $\alpha = 1$  in Algorithm 2, that is  $P^{(1)}$ , since it can help recover the eigenfunctions of the Laplace Beltrami operator on  $\mathcal{N}_s$  regardless of the sampling distribution. We write the estimated data representation as

$$\hat{\Theta}_1(x) = (\hat{\eta}_{1,m,n,t}(\phi), \dots, \hat{\eta}_{N,m,n,t}(\phi))$$

and

$$\hat{\Theta}_2(x) = (e^{-l\hat{\lambda}_{1,m,n,t}}\hat{\eta}_{1,m,n,t}(\phi), \dots, e^{-l\hat{\lambda}_{N,m,n,t}}\hat{\eta}_{N,m,n,t}(\phi)),$$

where  $x = T(\phi, \psi)$ ,  $(\hat{\lambda}_{l,m,n,t}, \hat{\eta}_{l,m,n,t})$  is the estimated eigenvalue and eigenfunction by  $P^{(1)}$  on  $m$  samples of  $n$ -views data. We also write the resulting  $k$ NN as  $\hat{h}_{\hat{\Theta}_1(X)}(x)$  and  $\hat{h}_{\hat{\Theta}_2(X)}(x)$  in this section. We need the following assumptions to study the performance of new data representation.

**Assumption 2.** *It holds that*

- (a) *Suppose  $f_v(\psi|\phi)$  is uniform distribution on  $\mathcal{M}(\phi)$  for any  $\phi$*
- (b) *There exists a constant  $\kappa$  such that  $1/\kappa < f_s(\phi) < \kappa$ , and  $f_s(\phi)$  is twice differentiable.*
- (c) *We choose  $t \asymp (\log m/m)^{2/(4d+13)}$*
- (d)  *$m$  is larger than a constant that relies on the smallest gap between the first  $N+1$  eigenvalues of  $\mathcal{L}_{\mathcal{N}_s}$ , i.e.,  $\min_{1 \leq l \leq N} |\lambda_{l+1} - \lambda_l|$ , the density  $f_s(\phi)$ , and the volume, injectivity radius, curvature of the manifolds  $\mathcal{M}$  and  $\mathcal{N}_s$ .*
- (e) *We assume there exists a  $u > d/2 + 13/4$  such that*

$$\sup_{y \in \mathcal{M}(\phi_i)} \left| \frac{1}{\text{Vol}\mathcal{N}_v} \int_{\mathcal{M}(\phi_{i'})} \exp\left(-\frac{\|x-y\|^2}{t}\right) dx - \tilde{h}_t(\phi_i, \phi_{i'}) \right| < C \tilde{h}_t(\phi_i, \phi_{i'}) t^u$$

$$\text{where } \tilde{h}_t(\phi_1, \phi_2) = \text{Vol}^{-2}\mathcal{N}_v \int_{\mathcal{M}(\phi_1)} \int_{\mathcal{M}(\phi_2)} \exp(-\|x-y\|^2/t) dx dy.$$

These assumptions are used to investigate the convergence rate of estimated eigenvalues and eigenvectors in the  $\ell_\infty$  norm. Similar assumptions also appear in proving the spectral convergence rate of diffusion maps (Dunson et al., 2021). We need the last assumption since the randomized kernel is used here. With these assumptions, the following proposition characterizes how fast the eigenvalues and eigenvectors estimated by  $P^{(1)}$  converge to the eigenvalues and eigenfunctions of  $\mathcal{L}_{\mathcal{N}_s}$ .

**Proposition 1.** *Suppose that the Assumption 2 holds. Let  $(\lambda_l, \eta_l(\phi))$  be the eigenvalues and eigenfunctions of  $\mathcal{L}_{\mathcal{N}_s}$  and  $(\lambda_{l,m,n,t}, \vec{\eta}_{l,m,n,t})$  be the eigenvalues and eigenvectors of  $(I - P^{(1)})/t$ . With probability at least  $1 - m^{-2}$ , there exist constants  $c_{\kappa,l}$  such that  $1/\kappa < c_{\kappa,l} < \kappa$ ,*

$$|\lambda_l - \lambda_{l,m,n,t}| \lesssim \left(\frac{\log m}{m}\right)^{3/(8d+26)}, \quad 1 \leq l \leq N,$$



and

$$|a_l c_{\kappa,l} [\vec{\eta}_{l,m,n,t}]_i - \eta_l(\phi_i)| \lesssim \left( \frac{\log m}{m} \right)^{1/(4d+13)}, \quad 1 \leq l \leq N, \quad 1 \leq i \leq m.$$

The convergence rate of eigenvalues presented in Proposition 1 is the same as the one in Dunson et al. (2021), while the convergence rate of eigenvectors is faster because we do not need to normalize the eigenvectors. Although it is unknown whether these convergence rates are sharp or not in our settings, they can help characterize the convergence rate of excess risk in  $\hat{h}_{\hat{\Theta}_1(X)}(x)$  and  $\hat{h}_{\hat{\Theta}_2(X)}(x)$ . The following theorem shows that the estimated data representations can improve  $k$ -NN if we have a large enough unlabeled augmented data set.

**Theorem 3.** *Suppose that the Assumption 1 and 2 hold, and  $\hat{\Theta}_1(x)$  and  $\hat{\Theta}_2(x)$  are estimated by  $m$  samples of  $n$ -views data. If we choose  $l$ ,  $N$ , and  $k$  in the same way as Theorem 2, then*

$$r(\hat{h}_{\hat{\Theta}_1(X)}) \lesssim (e^{d_s l_0 \lambda_{N_0} s})^{-\frac{\alpha(1+\beta)}{2\alpha+d_s}} + \left( \frac{\log m}{m} \right)^{\frac{\alpha(1+\beta)}{4d+13}} \quad \text{and} \quad r(\hat{h}_{\hat{\Theta}_2(X)}) \lesssim s^{-\frac{\alpha(1+\beta)}{2\alpha+d_s}} + \left( \frac{\log m}{m} \right)^{\frac{\alpha(1+\beta)}{4d+13}},$$

with probability at least  $1 - m^{-2}$ .

Theorem 3 suggests that the estimated data representation  $\hat{\Theta}_1(x)$  and  $\hat{\Theta}_2(x)$  can improve  $k$ -NN similarly to  $\Theta_1(x)$  and  $\Theta_2(x)$  when the sample size  $m$  is large enough. In particular, when  $m/\log m \gg s^{(4d+13)/(2\alpha+d_s)}$ , the convergence rates in Theorem 3 are the same as in Theorem 2.

## 4 A Computationally Efficient Formulation

Although the method proposed in Section 2 can help find augmentation invariant data representation, they pose practical challenges in generalizability and computational efficiency when applied to large data sets. The output of Algorithms 1 and 2 are just new representations of data points in the underlying data set. Nyström extension is one commonly used way to extend the representation to some new data point (Nyström, 1930). However, this way can be computationally expensive since the computational complexity of extending one new point is  $O(mN)$ . In addition, Algorithms 1 and 2 need to evaluate the pairwise distance

between any augmented data, so the computation complexity is at least  $O(m^2n^2)$ . Is it possible to develop a more generalizable and computationally efficient way for augmentation invariant manifold learning?

Motivated by recent works in HaoChen et al. (2021) and Balestriero and LeCun (2022), we borrow an idea from existing self-supervised learning methods. The idea is to parameterize the data representation maps and then apply modern optimization techniques to solve the problem. Specifically, let  $\Theta_\beta(x) : \mathcal{M} \rightarrow \mathbb{R}^N$  be a map with parameter  $\beta \in \mathcal{B}$ . For example, a deep neural network encoder is one of the most popular models for  $\Theta_\beta(x)$  in self-supervised learning methods (Chen et al., 2020b; Grill et al., 2020; Chen and He, 2021; Zbontar et al., 2021). With the parameterized representation  $\Theta_\beta(x)$ , the optimization problem in (3) can be rewritten as

$$\begin{aligned} \min_{\beta \in \mathcal{B}} \quad & \frac{1}{2} \sum_{i_1, i_2=1}^m \sum_{j_1, j_2=1}^n W_{i_1, j_1, i_2, j_2} \|\Theta_\beta(X_{i_1, j_1}) - \Theta_\beta(X_{i_2, j_2})\|^2 \\ \text{s.t.} \quad & \Theta_\beta(X_{i,1}) = \dots = \Theta_\beta(X_{i,n}), \quad 1 \leq i \leq m \\ & \sum_{i=1}^m \sum_{j=1}^n \Theta_{\beta, l_1}(X_{i,j}) \Theta_{\beta, l_2}(X_{i,j}) = \delta_{l_1, l_2}, \quad 1 \leq l_1, l_2 \leq N \end{aligned} \quad (4)$$

where  $\Theta_{\beta, l}(x)$  is the  $l$ th component of  $\Theta_\beta(x)$  and  $\delta_{l_1, l_2}$  is the Kronecker delta, that is,  $\delta_{l_1, l_2} = 1$  if  $l_1 = l_2$  and  $\delta_{l_1, l_2} = 0$  if  $l_1 \neq l_2$ . The last constraint is to enforce finding orthogonal eigenvectors.

To make the problem more computationally efficient, we can transform the above optimization problem in (4) into the following form

$$\min_{\beta \in \mathcal{B}} \quad \underbrace{\sum_{i=1}^m W_{i, i^-} \|\Theta_\beta(X_i) - \Theta_\beta(X_{i^-})\|^2}_{\text{unsupervised signal}} + \lambda_1 \underbrace{\sum_{i=1}^m \|\Theta_\beta(X_i) - \Theta_\beta(X_{i^+})\|^2}_{\text{self-supervised signal}} + \underbrace{\lambda_2 \mathcal{R}(\Theta_\beta)}_{\text{regularization}} \quad (5)$$

We now discuss the three parts of the above optimization problem in detail.

- **Unsupervised signal.** In the graph Laplacian, we need to evaluate weights between any pairs of data points, which is the most computationally intensive part. To overcome this issue, we adopt a sub-sampling strategy to approximate the graph Laplacian part. More concretely, if we consider random variables  $i' \sim \text{Unif}\{1, \dots, m\}$  and  $j, j' \sim$

Unif $\{1, \dots, n\}$ , then

$$\begin{aligned} & \frac{1}{m} \sum_{i=1}^m \mathbb{E}_{i',j,j'} (W_{i,j,i',j'} \|\Theta_\beta(X_{i,j}) - \Theta_\beta(X_{i',j'})\|^2) \\ &= \frac{1}{n^2 m^2} \sum_{i_1, i_2=1}^m \sum_{j_1, j_2=1}^n W_{i_1, j_1, i_2, j_2} \|\Theta_\beta(X_{i_1, j_1}) - \Theta_\beta(X_{i_2, j_2})\|^2 \end{aligned}$$

For simplicity, we write  $X_{i,j}$  as  $X_i$  if  $j$  is a realization of Unif $\{1, \dots, n\}$  and  $X_{i',j'}$  as  $X_{i-}$  if  $i'$  and  $j'$  are some realizations of Unif $\{1, \dots, m\}$  and Unif $\{1, \dots, n\}$ . Thus, we can expect

$$\frac{1}{m} \sum_{i=1}^m W_{i,i-} \|\Theta_\beta(X_i) - \Theta_\beta(X_{i-})\|^2 \approx \frac{1}{n^2 m^2} \sum_{i_1, i_2=1}^m \sum_{j_1, j_2=1}^n W_{i_1, j_1, i_2, j_2} \|\Theta_\beta(X_{i_1, j_1}) - \Theta_\beta(X_{i_2, j_2})\|^2.$$

Like the classical manifold learning methods, the unsupervised signal part tries to push the representations closer when the Euclidean distance between data points is smaller.

- **Self-supervised signal.** The constraint  $\Theta_\beta(X_{i,1}) = \dots = \Theta_\beta(X_{i,n})$  is designed to find augmentation invariant data representation. To convert a constrained problem into an unconstrained problem, we can replace this constraint with a penalty function

$$\lambda_1 \sum_{i=1}^m \left( \frac{2}{n(n-1)} \sum_{1 \leq j < j' \leq n} \|\Theta_\beta(X_{i,j}) - \Theta_\beta(X_{i,j'})\|^2 \right),$$

where  $\lambda_1$  is the tuning parameter. We can still apply a sub-sampling strategy to simplify the penalty function. Let  $X_i$  be the same data point as in the unsupervised signal part, and  $X_{i+}$  be another random data point from  $X_{i,1}, \dots, X_{i,n}$ . Hence, the penalty function can be approximated by

$$\lambda_1 \sum_{i=1}^m \|\Theta_\beta(X_i) - \Theta_\beta(X_{i+})\|^2.$$

This penalty function aims to push the augmented data of the same sample close to each other.

- **Regularization.** We consider another penalty function to enforce orthogonality of  $\Theta_\beta$  in an unconstrained problem

$$\lambda_2 \mathcal{R}(\Theta_\beta) = \lambda_2 \sum_{1 \leq l_1 \leq l_2 \leq N} \left( \sum_{i=1}^m \Theta_{\beta, l_1}(X_i) \Theta_{\beta, l_2}(X_i) - \delta_{l_1, l_2} \right)^2.$$

In this way, we can force the different components of  $\Theta_\beta$  to be orthogonal to each other. The regularization term is similar to the loss function in Barlow Twins (Zbontar et al., 2021).

Compared with the original problem (4), the problem in (5) is an unconstrained optimization problem with some simple structure so that we can apply some efficient optimization algorithms, such as stochastic gradient descent (Wright and Recht, 2022).

We now compare the loss function in (5) and the loss functions in existing self-supervised representation data learning methods (Chen et al., 2020b; Grill et al., 2020; Zbontar et al., 2021). Most self-supervised learning methods have a similar triplet data structure  $(X_i, X_{i+}, X_{i-})$  and aim to preserve the closeness between the augmented data of the same sample. There are also several key unique characteristics in our new loss function. First, the new loss function keeps the local similarity between the negative pair of data  $(X_i, X_{i-})$ , while the existing self-supervised learning methods either ignore the negative pair (in non-contrastive methods) or push the negative pair far from each other despite their Euclidean distance (in contrastive methods). Second, the regularization part in (5) can help avoid dimensional collapse observed in some self-supervised learning methods (Hua et al., 2021; Wen and Li, 2022). Third, the tuning parameters  $\lambda_1$  and  $\lambda_2$  help balance the unsupervised and self-supervised signals.

## 5 Numerical Experiments

In this section, we study the numerical performance of augmentation invariant manifold learning through a series of experiments. We conducted the numerical experiments on both simulated and handwritten digits data sets.

### 5.1 Simulated Data

To simulate the data, we consider three product manifolds: the first one is the torus used in the introduction (torus), that is,  $x = (x_1, x_2, x_3)$  such that  $x_1 = (10 + 5 \cos \phi) \cos \psi$ ,  $x_2 = (10 + 5 \cos \phi) \sin \psi$ , and  $x_3 = 5 \sin \phi$ , where  $\phi, \psi \in (0, 2\pi]$ ; the second one is the Swiss

roll in 3-dimensional space (Swiss roll 1), that is,  $x = (x_1, x_2, x_3)$  such that  $x_1 = \phi \cos \phi$ ,  $x_2 = \phi \sin \phi$ , and  $x_3 = \psi$ , where  $\phi \in (1.5\pi, 4.5\pi)$  and  $\psi \in (0, 10)$ ; the third one is the Swiss roll with changing role of  $\phi$  and  $\psi$  (Swiss roll 2), that is,  $x = (x_1, x_2, x_3)$  such that  $x_1 = \psi \cos \psi$ ,  $x_2 = \psi \sin \psi$ , and  $x_3 = \phi$ , where  $\phi \in (0, 10)$  and  $\psi \in (1.5\pi, 4.5\pi)$ . We follow the same procedure in Section 1.2 to generate multi-view augmented data, assuming the probability density functions  $f_s(\phi)$  and  $f_v(\psi|\phi)$  are uniform distribution. To recover the geometrical structure of  $\mathcal{N}_s$ , we apply three different augmentation invariant manifold learning methods: the Laplacian eigenmaps in Algorithm 1 ( $\hat{\Theta}_1$ ), the diffusion maps in Algorithm 2 with  $\alpha = 1/2$  and  $l = 0.1$  ( $\hat{\Theta}_2$ ), and the diffusion maps in Algorithm 2 with  $\alpha = 1$  and  $l = 0.1$  ( $\hat{\Theta}_3$ ). Figure 3 summarizes the 2-dimensional embedding by applying these three methods to the three different types of manifolds. From Figure 3, it is clear that all three different methods can recover the geometrical structure of  $\mathcal{N}_s$  very well.

Manifold	Data Representation	$s = 50$	$s = 100$	$s = 200$	$s = 300$
Torus	$\hat{h}_X$	0.423	0.380	0.301	0.274
	$\hat{h}_{\hat{\Theta}_1(X)}$	0.311	0.236	0.216	0.223
	$\hat{h}_{\hat{\Theta}_2(X)}$	0.306	0.232	0.218	0.221
	$\hat{h}_{\hat{\Theta}_3(X)}$	0.305	0.234	0.216	0.221
Swiss Roll	$\hat{h}_X$	0.437	0.438	0.435	0.440
	$\hat{h}_{\hat{\Theta}_1(X)}$	0.423	0.427	0.379	0.343
	$\hat{h}_{\hat{\Theta}_2(X)}$	0.432	0.421	0.364	0.347
	$\hat{h}_{\hat{\Theta}_3(X)}$	0.434	0.410	0.357	0.332

Table 1: Comparisons of different data representations on  $k$ -NN when sample size  $s$  is different. The misclassification error is reported in the table.

In the next simulation experiment, we study if the new data representation can help improve the downstream analysis. In particular, we focus on the classification on the manifold with the  $k$ -NN classifier. We consider two different product manifolds: the torus and Swiss roll 2 in the previous experiment and four data representations: the original data  $X$  and data representations estimated by  $\hat{\Theta}_1$ ,  $\hat{\Theta}_2$ , and  $\hat{\Theta}_3$  in the previous experiment. To generate

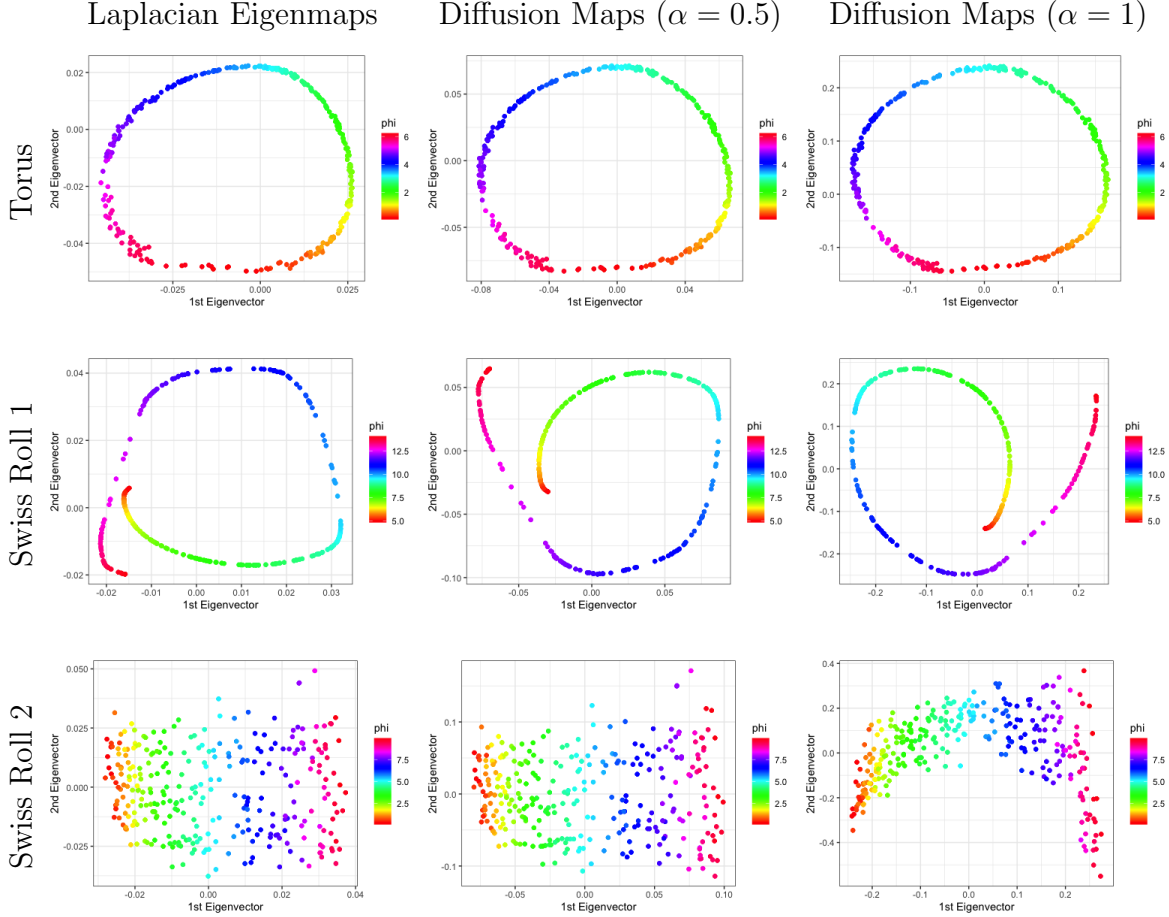


Figure 3: The embedding of three different product manifolds in  $\mathbb{R}^2$ . Different columns corresponds to different augmentation invariant manifold learning methods. All figures are colored by  $\phi$ .

the label  $Y$ , we assume the regression function is  $\gamma(x) = \mathbb{P}(Y = 1|X = x) = |\sin(\phi)|$  when  $x \in \mathcal{M}(\phi)$ . We vary the sample size of the training sets  $s = 50, 100, 200$ , and  $300$  and always choose the sample size in the testing set as  $100$ . The number of views in this simulation experiment is  $3$ , and the misclassification error is used as evaluation criteria. The results from  $100$  repeats of the simulation experiment are summarized in Table 1. Table 1 suggests that the new data representations can help improve  $k$ -NN, and the misclassification error is smaller when the sample size  $s$  is larger. In addition, the performance improved by three different representations are similar in Table 1.

In the last set of simulation experiments, we consider the effect of different regression

Data Representation	$\delta = 1$	$\delta = 2$	$\delta = 3$	$\delta = 4$
$\hat{h}_X$	0.267	0.400	0.430	0.425
$\hat{h}_{\hat{\Theta}_1(X)}$	0.208	0.226	0.242	0.280
$\hat{h}_{\hat{\Theta}_2(X)}$	0.207	0.222	0.244	0.273
$\hat{h}_{\hat{\Theta}_3(X)}$	0.211	0.223	0.243	0.275

Table 2: Comparisons of different data representations on  $k$ -NN when the regression function  $\gamma(x) = \mathbb{P}(Y = 1|X = x)$  is different. The misclassification error is reported in the table.

functions  $\gamma(x)$ . Specifically, we consider a similar setting to the previous simulation experiment. We only focus on the torus manifold with  $s = 300$  and choose the regression function as  $\gamma_\delta(x) = |\sin(\delta * \phi)|$  for  $\delta = 1, 2, 3, 4$  when  $x \in \mathcal{M}(\phi)$ . When  $\delta$  gets larger, the regression function becomes less smooth. We repeat the simulation 100 times and summarize the results in Table 2. Through Table 2, we can conclude that the classification problem gets more difficult when the regression is less smooths and the new data representation resulting from augmentation invariant manifold learning can also be helpful in the non-smooth case.

## 5.2 Handwritten Digits Data

We further study the performance of augmentation invariant manifold learning on the MNIST data set (LeCun et al., 1998). MNIST data set includes 60000 training images and 10000 testing images. All images are all  $28 \times 28$  gray-scale handwritten digits ranging from 0 to 9. This numerical experiment aims to compare the misclassification error of  $k$ -NN when different data representations are used. To apply augmentation invariant manifold learning, we consider two different ways of data augmentation: the first one is to resize the image to  $a \times a$  and then randomly crop it to  $28 \times 28$ , where  $a$  is a random number drawn from  $\{29, 30, 31, 32\}$ ; the second one is to rotate the image in  $b$  degree and then apply the same resizing and cropping as before, where  $b$  is a random number drawn between  $-10$  and  $10$ . The second data argumentation is more complex than the first one. Figure 4 illustrates these two ways of data augmentation on the image of a handwritten digit.

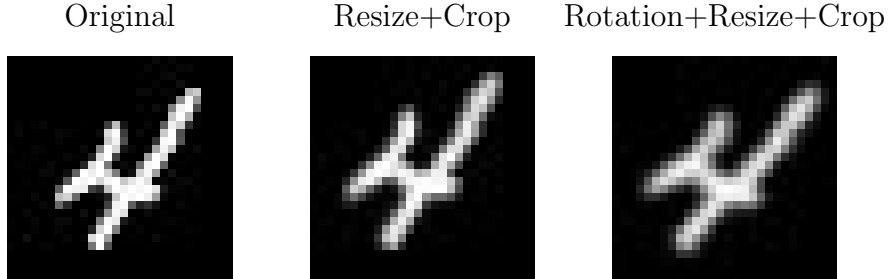


Figure 4: An example of augmented data in MNIST data set: from left to right are original, resize+crop, and rotation+resize+crop.

In this numerical experiment, we consider three different data representations: the original data  $X$ , the data representation  $\hat{\Theta}(X)$  learned from augmentation invariant Laplacian eigenmaps in Algorithm 1, and the data representation  $\hat{\Theta}_\beta(X)$  learned from the optimization problem (5) when  $\Theta_\beta$  is a deep neutral network encoder. To find the data representation  $\hat{\Theta}(X)$ , we randomly draw 1000 unlabeled images from the 60000 training images and apply the data augmentation operator on each image 7 times in augmentation invariant Laplacian eigenmaps. In  $\hat{\Theta}_\beta(X)$ , we consider a standard convolutional neural network encoder (2 convolution+relu layers, 2 pooling layers, and a fully connected layer) as the encoder (LeCun et al., 2015; Goodfellow et al., 2016) and choose the tuning parameter  $\lambda_1 = 100$  and  $\lambda_2 = 200$ . Due to its computational efficiency,  $\hat{\Theta}_\beta(X)$  is trained on 60000 unlabeled images in the training set.

Data Argumentation	Data Representation	$s = 50$	$s = 100$	$s = 200$	$s = 400$
No Augmentation	$X$	46.57%	34.48%	25.43%	18.56%
Resize+Crop	$\hat{\Theta}(X)$	45.82%	33.02%	24.27%	17.92%
Rotation+Resize+Crop		45.04%	32.86%	23.75%	17.59%
Resize+Crop	$\hat{\Theta}_\beta(X)$	44.18%	28.03%	19.51%	16.83%
Rotation+Resize+Crop		44.12%	27.19%	19.13%	16.71%

Table 3: Comparisons of different data augmentation and data representations on handwritten digits classification. The misclassification error is reported in the table.



We randomly draw  $s = 50, 100, 200, 400$  labeled images from the 60000 training images as our training data set to compare different data representations. The misclassification error is estimated on 100 images randomly drawn from testing images. For each sample size  $s$ , we repeat the experiments 100 times. Table 3 reports the average misclassification error resulting from different data representations. In Table 3, we observe that the new data representations learned by augmentation invariant manifold learning can help improve  $k$ -NN, and a more complex data augmentation is more helpful in downstream analysis. It is also interesting to note that the data representation learned from a larger data set can help improve downstream analysis more. All observations are consistent with our theoretical results.

## 6 Concluding Remarks

In this paper, we introduce a new product manifold model for data augmentation and theoretically characterize the role of data augmentation in self-supervised learning. Under the newly proposed model, the regression function defined on the product manifold can be decomposed into two parts

$$\gamma(x) = \tilde{\gamma}(T_{\pi}^{-1}(x)), \quad x \in \mathcal{M}.$$

Here,  $T_{\pi}^{-1}(x) = \pi(T^{-1}(x)) = \phi_x$  is a projection function that maps  $x$  to  $\phi_x$  when  $x \in \mathcal{M}(\phi_x)$ , where  $\pi(\phi, \psi) = \phi$  is a projection function on the product manifold. The augmentation invariant manifold learning tries to estimate  $T_{\pi}^{-1}(x)$  (or an equivalent one) from the unlabeled augmented data. When  $T_{\pi}^{-1}(x)$  can be estimated accurately, it is sufficient to estimate a  $d_s$ -dimensional function  $\tilde{\gamma}(\phi)$  instead of a high dimensional function  $\gamma(x)$  in the downstream analysis. This explains why the augmentation invariant manifold learning can help improve  $k$ -NN in the downstream analysis.

In augmentation invariant manifold learning, several tuning parameters exist, including bandwidth  $t$ , number of eigenvectors  $N$ , and the parameters  $\alpha, l$  in Algorithm 2. The theoretical analysis provides some recommendations for these tuning parameters' choices, but it is still a challenging job to select appropriate ones for the best empirical performance. Al-

though some data-driven methods are proposed for bandwidth  $t$  in classical manifold learning (Ding and Wu, 2020), these methods cannot directly apply to the augmentation invariant manifold learning. Hence, it could be interesting to develop an automatic way to choose these tuning parameters in future work. To simplify the theoretical analysis, we assume this paper’s conditional distribution  $f_v(\psi|\phi)$  is uniform. The theoretical analysis can also be extended to cases where the conditional distribution  $f_v(\psi|\phi)$  is not uniform, but  $\phi$  is independent of  $\psi$ . It is unclear if the proposed augmentation invariant manifold learning works when  $\phi$  and  $\psi$  are dependent, and we leave it as the future work.

## Acknowledgment

This project is supported by grants from the National Science Foundation (DMS-2113458).

## References

- N. S. Altman. An introduction to kernel and nearest-neighbor nonparametric regression. *The American Statistician*, 46(3):175–185, 1992.
- S. Arora, H. Khandeparkar, M. Khodak, O. Plevrakis, and N. Saunshi. A theoretical analysis of contrastive unsupervised representation learning. *arXiv preprint arXiv:1902.09229*, 2019.
- K. E. Atkinson. The numerical solution of the eigenvalue problem for compact integral operators. *Transactions of the American Mathematical Society*, 129(3):458–465, 1967.
- J. Audibert and A. B. Tsybakov. Fast learning rates for plug-in classifiers. *The Annals of statistics*, 35(2):608–633, 2007.
- R. Balestrierio and Y. LeCun. Contrastive and non-contrastive self-supervised learning recover global and local spectral embedding methods. *arXiv preprint arXiv:2205.11508*, 2022.

- J. Bates. The embedding dimension of laplacian eigenfunction maps. *Applied and Computational Harmonic Analysis*, 37(3):516–530, 2014.
- M. Belkin and P. Niyogi. Laplacian eigenmaps for dimensionality reduction and data representation. *Neural computation*, 15(6):1373–1396, 2003.
- M. Belkin and P. Niyogi. Towards a theoretical foundation for laplacian-based manifold methods. *Journal of Computer and System Sciences*, 74(8):1289–1308, 2008.
- Y. Bengio, A. Courville, and P. Vincent. Representation learning: A review and new perspectives. *IEEE transactions on pattern analysis and machine intelligence*, 35(8):1798–1828, 2013.
- T. Berry and J. Harlim. Iterated diffusion maps for feature identification. *Applied and Computational Harmonic Analysis*, 45(1):84–119, 2018.
- G. Biau and L. Devroye. *Lectures on the nearest neighbor method*, volume 246. Springer, 2015.
- M. Caron, I. Misra, J. Mairal, P. Goyal, P. Bojanowski, and A. Joulin. Unsupervised learning of visual features by contrasting cluster assignments. *Advances in Neural Information Processing Systems*, 33:9912–9924, 2020.
- K. Chan, Y. Yu, C. You, H. Qi, J. Wright, and Y. Ma. Redunet: A white-box deep network from the principle of maximizing rate reduction. *arXiv preprint arXiv:2105.10446*, 2021.
- S. Chen, E. Dobriban, and J. H. Lee. A group-theoretic framework for data augmentation. *Journal of Machine Learning Research*, 21:1–71, 2020a.
- T. Chen, S. Kornblith, M. Norouzi, and G. Hinton. A simple framework for contrastive learning of visual representations. In *International conference on machine learning*, pages 1597–1607. PMLR, 2020b.
- X. Chen and K. He. Exploring simple siamese representation learning. In *Proceedings of the IEEE/CVF Conference on Computer Vision and Pattern Recognition*, pages 15750–15758, 2021.

- H. Chereda, A. Bleckmann, F. Kramer, A. Leha, and T. Beissbarth. Utilizing molecular network information via graph convolutional neural networks to predict metastatic event in breast cancer. In *GMDS*, pages 181–186, 2019.
- Y. Chung and W. Weng. Learning deep representations of medical images using siamese cnns with application to content-based image retrieval. *arXiv preprint arXiv:1711.08490*, 2017.
- R. R. Coifman and S. Lafon. Diffusion maps. *Applied and Computational Harmonic Analysis*, 21(1):5–30, 2006.
- R. Collobert, J. Weston, L. Bottou, M. Karlen, K. Kavukcuoglu, and P. Kuksa. Natural language processing (almost) from scratch. *Journal of machine learning research*, 12: 2493–2537, 2011.
- J. Devlin, M. Chang, K. Lee, and K. Toutanova. Bert: Pre-training of deep bidirectional transformers for language understanding. In *Proceedings of the 2019 Conference of the North American Chapter of the Association for Computational Linguistics: Human Language Technologies*, pages 4171–4186, 2019.
- X. Ding and H. Wu. Impact of signal-to-noise ratio and bandwidth on graph laplacian spectrum from high-dimensional noisy point cloud. *arXiv preprint arXiv:2011.10725*, 2020.
- D. L. Donoho and C. Grimes. Hessian eigenmaps: Locally linear embedding techniques for high-dimensional data. *Proceedings of the National Academy of Sciences*, 100(10): 5591–5596, 2003.
- D. B. Dunson, H. Wu, and N. Wu. Spectral convergence of graph laplacian and heat kernel reconstruction in  $L^\infty$  from random samples. *Applied and Computational Harmonic Analysis*, 55:282–336, 2021.
- E. Fix. *Discriminatory analysis: nonparametric discrimination, consistency properties*, volume 1. USAF school of Aviation Medicine, 1985.

- S. Gidaris, P. Singh, and N. Komodakis. Unsupervised representation learning by predicting image rotations. In *International Conference on Learning Representations*, 2018.
- I. Goodfellow, Y. Bengio, and A. Courville. *Deep learning*. MIT press, 2016.
- J. Grill, F. Strub, F. Alché, C. Tallec, P. Richemond, E. Buchatskaya, C. Doersch, B. Avila Pires, Z. Guo, M. Gheshlaghi Azar, B. Piot, K. Kavukcuoglu, R. Munos, and M. Valko. Bootstrap your own latent—a new approach to self-supervised learning. *Advances in Neural Information Processing Systems*, 33:21271–21284, 2020.
- F. Gustafsson. *Statistical sensor fusion*. Studentlitteratur, 2010.
- I. Guyon, S. Gunn, M. Nikravesh, and L. A. Zadeh. *Feature extraction: foundations and applications*, volume 207. Springer, 2008.
- J. Z. HaoChen, C. Wei, A. Gaidon, and T. Ma. Provable guarantees for self-supervised deep learning with spectral contrastive loss. *Advances in Neural Information Processing Systems*, 34, 2021.
- K. He, H. Fan, Y. Wu, S. Xie, and R. Girshick. Momentum contrast for unsupervised visual representation learning. In *Proceedings of the IEEE/CVF conference on computer vision and pattern recognition*, pages 9729–9738, 2020.
- G. E. Hinton and R. Zemel. Autoencoders, minimum description length and helmholtz free energy. *Advances in neural information processing systems*, 6, 1993.
- R. D. Hjelm, A. Fedorov, S. Lavoie-Marchildon, K. Grewal, P. Bachman, A. Trischler, and Y. Bengio. Learning deep representations by mutual information estimation and maximization. In *International Conference on Learning Representations*, 2018.
- T. Hua, W. Wang, Z. Xue, S. Ren, Y. Wang, and H. Zhao. On feature decorrelation in self-supervised learning. In *Proceedings of the IEEE/CVF International Conference on Computer Vision*, pages 9598–9608, 2021.

- L. Jing and Y. Tian. Self-supervised visual feature learning with deep neural networks: A survey. *IEEE transactions on pattern analysis and machine intelligence*, 43(11):4037–4058, 2020.
- I. T. Jolliffe. *Principal component analysis*. Springer, 2002.
- M. Kim, C. Yan, D. Yang, Q. Wang, J. Ma, and G. Wu. Deep learning in biomedical image analysis. In *Biomedical Information Technology*, pages 239–263. Elsevier, 2020.
- D. Lahat, T. Adali, and C. Jutten. Multimodal data fusion: an overview of methods, challenges, and prospects. *Proceedings of the IEEE*, 103(9):1449–1477, 2015.
- Y. LeCun, L. Bottou, Y. Bengio, and P. Haffner. Gradient-based learning applied to document recognition. *Proceedings of the IEEE*, 86(11):2278–2324, 1998.
- Y. LeCun, Y. Bengio, and G. Hinton. Deep learning. *nature*, 521(7553):436–444, 2015.
- R. R. Lederman and R. Talmon. Learning the geometry of common latent variables using alternating-diffusion. *Applied and Computational Harmonic Analysis*, 44(3):509–536, 2018.
- O. Lindenbaum, A. Yeredor, M. Salhov, and A. Averbuch. Multi-view diffusion maps. *Information Fusion*, 55:127–149, 2020.
- E. J. Nyström. Über die praktische auflösung von integralgleichungen mit anwendungen auf randwertaufgaben. *Acta Mathematica*, 54:185–204, 1930.
- P. Petersen. *Riemannian geometry*, volume 171. Springer, 2006.
- P. Pope, C. Zhu, A. Abdelkader, M. Goldblum, and T. Goldstein. The intrinsic dimension of images and its impact on learning. *arXiv preprint arXiv:2104.08894*, 2021.
- J. W. Portegies. Embeddings of riemannian manifolds with heat kernels and eigenfunctions. *Communications on Pure and Applied Mathematics*, 69(3):478–518, 2016.

- S. Rhee, S. Seo, and S. Kim. Hybrid approach of relation network and localized graph convolutional filtering for breast cancer subtype classification. In *Proceedings of the 27th International Joint Conference on Artificial Intelligence*, pages 3527–3534, 2018.
- S. T. Roweis and L. K. Saul. Nonlinear dimensionality reduction by locally linear embedding. *science*, 290(5500):2323–2326, 2000.
- M. Salhov, O. Lindenbaum, Y. Aizenbud, A. Silberschatz, Y. Shkolnisky, and A. Averbuch. Multi-view kernel consensus for data analysis. *Applied and Computational Harmonic Analysis*, 49(1):208–228, 2020.
- R. J. Samworth. Optimal weighted nearest neighbour classifiers. *The Annals of Statistics*, 40(5):2733–2763, 2012.
- C. Shorten and T. M. Khoshgoftaar. A survey on image data augmentation for deep learning. *Journal of big data*, 6(1):1–48, 2019.
- A. Singer and H. Wu. Vector diffusion maps and the connection laplacian. *Communications on pure and applied mathematics*, 65(8):1067–1144, 2012.
- M. Talagrand. *Upper and lower bounds for stochastic processes*, volume 60. Springer, 2014.
- R. Talmon and H. Wu. Latent common manifold learning with alternating diffusion: analysis and applications. *Applied and Computational Harmonic Analysis*, 47(3):848–892, 2019.
- J. B. Tenenbaum, V. Silva, and J. C. Langford. A global geometric framework for nonlinear dimensionality reduction. *science*, 290(5500):2319–2323, 2000.
- Y. Tian, D. Krishnan, and P. Isola. Contrastive multiview coding. In *European conference on computer vision*, pages 776–794. Springer, 2020a.
- Y. Tian, L. Yu, X. Chen, and S. Ganguli. Understanding self-supervised learning with dual deep networks. *arXiv preprint arXiv:2010.00578*, 2020b.
- C. Tosh, A. Krishnamurthy, and D. Hsu. Contrastive learning, multi-view redundancy, and linear models. In *Algorithmic Learning Theory*, pages 1179–1206. PMLR, 2021.

- Y. Tsai, Y. Wu, R. Salakhutdinov, and L. Morency. Self-supervised learning from a multi-view perspective. *arXiv preprint arXiv:2006.05576*, 2020.
- U. Von Luxburg, M. Belkin, and O. Bousquet. Consistency of spectral clustering. *The Annals of Statistics*, pages 555–586, 2008.
- S. Wang. Self-supervised metric learning in multi-view data: A downstream task perspective. *Journal of the American Statistical Association*, (just-accepted):1–41, 2022.
- S. Wang, J. Fan, G. Pocock, E. T. Arena, K. W. Eliceiri, and M. Yuan. Structured correlation detection with applications to colocalization analysis in dual-channel fluorescence microscopic imaging. *Statistica Sinica*, 31:333–360, 2021.
- C. Wei, K. Shen, Y. Chen, and T. Ma. Theoretical analysis of self-training with deep networks on unlabeled data. *arXiv preprint arXiv:2010.03622*, 2020.
- K. Q. Weinberger and L. K. Saul. Unsupervised learning of image manifolds by semidefinite programming. *International journal of computer vision*, 70(1):77–90, 2006.
- Z. Wen and Y. Li. Toward understanding the feature learning process of self-supervised contrastive learning. In *International Conference on Machine Learning*, pages 11112–11122. PMLR, 2021.
- Z. Wen and Y. Li. The mechanism of prediction head in non-contrastive self-supervised learning. *arXiv preprint arXiv:2205.06226*, 2022.
- S. J. Wright and B. Recht. *Optimization for data analysis*. Cambridge University Press, 2022.
- J. Zbontar, L. Jing, I. Misra, Y. LeCun, and S. Deny. Barlow twins: Self-supervised learning via redundancy reduction. In *International Conference on Machine Learning*, pages 12310–12320. PMLR, 2021.
- Z. Zhang and H. Zha. Principal manifolds and nonlinear dimensionality reduction via tangent space alignment. *SIAM journal on scientific computing*, 26(1):313–338, 2004.



## Appendix A Augmentation Invariant Diffusion Maps

This section presents an augmentation invariant version of diffusion maps, summarized in Algorithm 2. A similar argument in Theorem 1 makes it sufficient to study the corresponding continuous version of Algorithm 2. Following the notation in the proof of Theorem 1, we define a weighted kernel for given  $\alpha$

$$\tilde{h}_t^{(\alpha)}(\phi_1, \phi_2) = \frac{\tilde{h}_t(\phi_1, \phi_2)}{f_{s,t}^\alpha(\phi_1)f_{s,t}^\alpha(\phi_2)}, \quad \text{where } f_{s,t}(\phi_1) = \int \tilde{h}_t(\phi_1, \phi_2)f_s(\phi_2)d\phi_2.$$

Then, the operator for a continuous version of Algorithm 2 is defined as

$$\mathcal{P}_{t,\alpha}g(\phi_1) = \int \frac{\tilde{h}_t^{(\alpha)}(\phi_1, \phi_2)}{D_t^{(\alpha)}(\phi_1)}g(\phi_2)f_s(\phi_2)d\phi_2, \quad \text{where } D_t^{(\alpha)}(\phi_1) = \int \tilde{h}_t^{(\alpha)}(\phi_1, \phi_2)f_s(\phi_2)d\phi_2,$$

where  $g(\phi)$  is a function defined on  $\mathcal{N}_s$ . The following theorem characterizes the asymptotic behavior of operator  $\mathcal{P}_{t,\alpha}$ .

**Theorem 4.** *Define  $L_{t,\alpha} = (I - \mathcal{P}_{t,\alpha})/t$ . Then we can show that*

$$\lim_{t \rightarrow 0} L_{t,\alpha}g = \frac{\mathcal{L}_{\mathcal{N}_s}(gf_s^{1-\alpha})}{f_s^{1-\alpha}} - \frac{\mathcal{L}_{\mathcal{N}_s}(f_s^{1-\alpha})}{f_s^{1-\alpha}}g,$$

where  $\mathcal{L}_{\mathcal{N}_s}$  is Laplace Beltrami operator on  $\mathcal{N}_s$  and  $g(\phi)$  is a function defined on  $\mathcal{N}_s$ .

We omit the proof here as the same arguments in Coifman and Lafon (2006) still hold if we have Lemma 9. The result suggests we can always choose  $\alpha = 1$  to recover the Laplace Beltrami operator on  $\mathcal{N}_s$ .

## Appendix B Proof

In this section,  $C$  and  $c$  refer to some generic constant relying on the properties of manifold, which can be different at different places.

### B.1 Proof of Theorem 1

In Algorithm 1, the integrated weight  $W_n(\phi_i, \phi_{i'})$  can be seen a noisy version of the following weight, that is a kernel defined on  $\mathcal{N}_s$

$$\tilde{h}_t(\phi_1, \phi_2) = \frac{1}{\text{Vol}^2\mathcal{N}_v} \int_{\mathcal{M}(\phi_1)} \int_{\mathcal{M}(\phi_2)} \exp\left(-\frac{\|x-y\|^2}{t}\right) dx dy,$$

---

**Algorithm 2** Augmentation Invariant Diffusion Maps
 

---

**Input:** A set of augmented data:  $(X_{i,1}, \dots, X_{i,n})$ ,  $1 \leq i \leq m$  and the parameters  $\alpha$  and  $l$ .

Step 1: Calculate the weights between samples

$$W_{i_1, i_2} = \frac{1}{n^2} \sum_{j_1, j_2=1}^n \exp\left(-\frac{\|X_{i_1, j_1} - X_{i_2, j_2}\|^2}{t}\right), \quad i_1, i_2 = 1, \dots, m.$$

Step 2: Normalize the weight matrix  $W^{(\alpha)} = D^{-\alpha} W D^{-\alpha}$ , where  $D$  is a diagonal degree matrix of  $W$ , i.e.  $D_{i,i} = \sum_j W_{i,j}$ .

Step 3: Evaluate the transition matrix  $P^{(\alpha)} = (D^{(\alpha)})^{-1} W^{(\alpha)}$ , where  $D^{(\alpha)}$  is a diagonal degree matrix of  $W^{(\alpha)}$ .

Step 4: Find the first  $N$  eigenvectors and eigenvalues of  $P^{(\alpha)}$ , name them  $\vec{\eta}_1, \dots, \vec{\eta}_N$  and  $\lambda_1, \dots, \lambda_N$ .

**Output:** The representation for each sample:  $(X_{i,1}, \dots, X_{i,n}) \rightarrow (e^{-l\lambda_1} \eta_{1,i}, \dots, e^{-l\lambda_N} \eta_{N,i})$

---

where  $\mathcal{M}(\phi) = \{x : x = T(\phi, \psi), \forall \psi \in \mathcal{N}_v\}$ . We define a continuous version of operator  $L_{m,n}^t g(\phi)$

$$L_{f_s}^t g(\phi_1) = \frac{1}{t} \int_{\mathcal{N}_s} \frac{\tilde{h}_t(\phi_1, \phi_2)}{\sqrt{D^t(\phi_1)} \sqrt{D^t(\phi_2)}} (g(\phi_1) - g(\phi_2)) f_s(\phi_2) d\phi_2,$$

where  $D^t(\phi)$  is defined as

$$D^t(\phi) = \int_{\mathcal{N}_s} \tilde{h}_t(\phi, \phi') f_s(\phi') d\phi'.$$

The rest of proof is divided into two steps: 1) we show  $L_{f_s}^t$  converges to  $\mathcal{L}_{\mathcal{N}_s, f_s}$  when  $t \rightarrow 0$ ; 2) apply concentration inequality to show  $L_{m,n}^t$  converges to  $L_{f_s}^t$ .

**Step 1** For a function  $g(\phi)$  defined on  $\mathcal{N}_s$ , we define

$$G_t g(\phi) = \frac{1}{t^{d/2}} \int_{\mathcal{N}_s} \tilde{h}_t(\phi, \phi') g(\phi') d\phi'.$$

Clearly, the definition suggests  $t^{-d/2} D^t(\phi) = G_t f_s(\phi)$  so Lemma 9 leads to

$$t^{-d/2} D^t(\phi) = m_0 f_s(\phi) - t \frac{m_2}{2} \mathcal{L}_{\mathcal{N}_s} f_s(\phi) + O(t^2).$$

Consequently, we have

$$\frac{1}{\sqrt{t^{-d/2} D^t(\phi)}} = \frac{1}{\sqrt{m_0 f_s(\phi)}} \left( 1 + t \frac{m_2}{4m_0} \frac{\mathcal{L}_{\mathcal{N}_s} f_s(\phi)}{f_s(\phi)} + O(t^2) \right).$$

Plug in the above to the definition of  $L_{f_s}^t g(\phi)$  and we obtain

$$\begin{aligned}
L_{f_s}^t g(\phi_1) &= \frac{1}{t} \int_{\mathcal{N}_s} \frac{\tilde{h}_t(\phi_1, \phi_2)/t^{d/2}}{m_0 \sqrt{f_s(\phi_1)} \sqrt{f_s(\phi_2)}} (g(\phi_1) - g(\phi_2)) f_s(\phi_2) (1 + O(t)) d\phi_2 \\
&= \frac{1 + O(t)}{t} \frac{1}{m_0 \sqrt{f_s(\phi_1)}} G_t r(\phi_1) \\
&= \frac{1 + O(t)}{t} \frac{1}{m_0 \sqrt{f_s(\phi_1)}} \left( m_0 r(\phi_1) - t \frac{m_2}{2} \mathcal{L}_{\mathcal{N}_s} r(\phi_1) + O(t^2) \right) \\
&= (1 + O(t)) \frac{1}{m_0 \sqrt{f_s(\phi_1)}} \left( -\frac{m_2}{2} \left( -\sqrt{f_s(\phi_1)} \mathcal{L}_{\mathcal{N}_s} g(\phi_1) - 2 \langle \nabla g, \nabla \sqrt{f_s} \rangle \right) + O(t) \right) \\
&= \frac{1}{2} \left( \mathcal{L}_{\mathcal{N}_s} g(\phi_1) + \frac{1}{f_s(\phi_1)} \langle \nabla g, \nabla f_s \rangle \right) + O(t)
\end{aligned}$$

Here, we define  $r(\phi) = (g(\phi_1) - g(\phi)) \sqrt{f_s(\phi)}$ , use the fact  $\mathcal{L}(fg) = f\mathcal{L}g + g\mathcal{L}f + 2\langle \nabla f, \nabla g \rangle$  and apply Lemma 9 again. So we complete the proof for  $L_{f_s}^t g(\phi) = \mathcal{L}_{\mathcal{N}_s, f_s} g(\phi)/2 + O(t)$ .

**Step 2** We define an intermediate operator

$$\tilde{L}_{m,n}^t g(\phi) = \frac{1}{m} \sum_{i=1}^m \frac{1}{t} \frac{W_n(\phi_i, \phi)}{\sqrt{D^t(\phi)} \sqrt{D^t(\phi_i)}} (g(\phi) - g(\phi_i)).$$

We write  $\mathbf{X}_i = (X_{i,1}, \dots, X_{i,n})$  and know that there exist a constant  $C_g$  such that

$$\frac{1}{t} \frac{W_n(\phi_i, \phi)}{\sqrt{D^t(\phi)} \sqrt{D^t(\phi_i)}} (g(\phi) - g(\phi_i)) \leq \frac{C_g}{t^{(d+2)/2}}.$$

Thus, an application of Hoeffding's inequality suggests

$$\mathbb{P} \left( |\tilde{L}_{m,n}^t g(\phi) - L_{f_s}^t g(\phi)| > \epsilon \right) \leq 2 \exp(-c_g m t^{d+2} \epsilon^2),$$

where  $c_g$  is some constant depending on  $C_g$ . If we define the event

$$\mathcal{A}_1 = \left\{ |\tilde{L}_{m,n}^t g(\phi) - L_{f_s}^t g(\phi)| > \frac{r_m}{\sqrt{c_g m t^{d+2}}} \right\},$$

we can know  $\mathbb{P}(\mathcal{A}_1) \rightarrow 0$  if  $r_m \rightarrow \infty$ . For any given  $\phi$ , we apply Hoeffding's inequality to have

$$\mathbb{P} \left( |D_{m,n}^t(\phi) - D^t(\phi)| > \epsilon \right) \leq 2 \exp(-2m t^d \epsilon^2).$$

We apply union bound to yield

$$\mathbb{P} \left( \sup_{1 \leq i \leq m} |D_{m,n}^t(\phi_i) - D^t(\phi_i)| > \epsilon \right) \leq 2m \exp(-2m t^d \epsilon^2).$$

We define another event

$$\mathcal{A}_2 = \left\{ \sup_{1 \leq i \leq m} |D_{m,n}^t(\phi_i) - D^t(\phi_i)| > \frac{\log m}{\sqrt{2mt^d}} \right\}$$

and know  $\mathbb{P}(\mathcal{A}_2) \rightarrow 0$ . Conditioned on the event  $\mathcal{A}_1^c \cap \mathcal{A}_2^c$ , we can have

$$\begin{aligned} |L_{m,n}^t g(\phi) - L_{f_s}^t g(\phi)| &\leq |L_{m,n}^t g(\phi) - \tilde{L}_{m,n}^t g(\phi)| + |\tilde{L}_{m,n}^t g(\phi) - L_{f_s}^t g(\phi)| \\ &\leq \frac{r_m}{\sqrt{c_g m t^{d+2}}} + \frac{\log m}{\sqrt{2mt^d}} \end{aligned}$$

Since we take  $t = m^{-1/(d+4)}$ , we can know that

$$\mathbb{P} \left( |L_{m,n}^t g(\phi) - L_{f_s}^t g(\phi)| > C \frac{r_m}{\sqrt{m t^{d+2}}} \right) \rightarrow 0.$$

We complete the proof.

## B.2 Proof of Theorem 2

### B.2.1 Proof for $\hat{h}_X$

We write  $\hat{\gamma}(x) = k^{-1} \sum_{i=1}^k \mathbf{I}(Y_{(i)} = 1)$  and  $\hat{\gamma}^*(x) = k^{-1} \sum_{i=1}^k \gamma(X_{(i)})$ . If we apply Hoeffding's inequality, then we know that

$$\mathbb{P}(|\hat{\gamma}(x) - \hat{\gamma}^*(x)| > t) = \mathbb{P} \left( \frac{1}{k} \left| \sum_{i=1}^k (\mathbf{I}(Y_{(i)} = 1) - \gamma(X_{(i)})) \right| > t \right) \leq 2e^{-2kt^2}.$$

We write the ball defined by Euclidean distance as  $\mathcal{B}(x, r, \|\cdot\|) = \{y \in \mathcal{M} : \|x - y\| \leq r\}$  and  $r_a$  as the radius such that  $\mu(\mathcal{B}(x, r_a, \|\cdot\|)) = a$ . Here  $\mu$  is the probability of  $X$  on  $\mathcal{M}$ . By Chernoff bound, we have

$$\mathbb{P}(\|X_{(k+1)} - x\| > r_{2k/s}) = \mathbb{P} \left( \sum_{i=1}^s \mathbf{I}(X_i \in \mathcal{B}(x, r_{2k/s}, \|\cdot\|)) \leq k \right) \leq e^{-k/6}.$$

Next, we can work on the largest difference  $\sup_{y \in \mathcal{B}(x, r_{2k/s}, \|\cdot\|)} |\gamma(y) - \gamma(x)|$ . Because  $\|x - y\| \leq d_{\mathcal{M}}(x, y)$ , we can know that

$$\mathcal{B}(x, r_{2k/s}, d_{\mathcal{M}}) \subset \mathcal{B}(x, r_{2k/s}, \|\cdot\|),$$

where  $d_{\mathcal{M}}$  is Riemannian distance on the manifold  $\mathcal{M}$  and  $\mathcal{B}(x, r, d_{\mathcal{M}}) = \{y \in \mathcal{M} : d_{\mathcal{M}}(x, y) \leq r\}$ . By the Bishop-Gromov inequality (Petersen, 2006), we can know that

$$\text{Vol}\mathcal{B}(x, r_{2k/s}, d_{\mathcal{M}}) \geq w_d r_{2k/s}^d,$$

where  $\text{Vol}$  is the volume on the manifold  $\mathcal{M}$  and  $w_d r^d$  is the volume of Euclidean ball of radius  $r$ . Since the probability density function is lower bounded, we can know that

$$w_d r_{2k/s}^d \leq \text{Vol}\mathcal{B}(x, r_{2k/s}, \|\cdot\|) \leq \frac{1}{f_{\min}} \mu(\mathcal{B}(x, r_{2k/s}, \|\cdot\|)) = \frac{2k}{f_{\min} s}.$$

Thus, we can conclude that  $r_{2k/s} \leq C(k/s)^{1/d}$ . By Lemma 4.3 in Belkin and Niyogi (2008), we can know that  $d_{\mathcal{M}}(x, y) \leq r_{2k/s}(1 + Cr_{2k/s})$  if  $y \in \mathcal{B}(x, r_{2k/s}, \|\cdot\|)$ , which immediately leads to  $d_{\mathcal{M}}(x, y) \leq C(k/s)^{1/d}$  when  $y \in \mathcal{B}(x, r_{2k/s}, \|\cdot\|)$ . Since  $\mathcal{M} = T(\mathcal{N}_s \times \mathcal{N}_v)$  where  $T$  is an isometry, we have

$$|\gamma(y) - \gamma(x)| = |\tilde{\gamma}(\phi_y) - \tilde{\gamma}(\phi_x)| \leq Ld_{\mathcal{N}_s}(\phi_x, \phi_y)^\alpha \leq Ld_{\mathcal{M}}(x, y)^\alpha \leq C(k/s)^{\alpha/d},$$

where  $y \in \mathcal{B}(x, r_{2k/s}, \|\cdot\|)$ ,  $x \in \mathcal{M}(\phi_x)$ , and  $y \in \mathcal{M}(\phi_y)$ . Therefore, we can know

$$\mathbb{P}\left(|\hat{\gamma}^*(x) - \gamma(x)| > C\left(\frac{k}{s}\right)^{\alpha/d}\right) \leq e^{-k/6}.$$

Putting  $|\hat{\gamma}(x) - \hat{\gamma}^*(x)|$  and  $|\hat{\gamma}^*(x) - \gamma(x)|$  together yields

$$\mathbb{P}\left(|\hat{\gamma}(x) - \gamma(x)| > t + C\left(\frac{k}{s}\right)^{\alpha/d}\right) \leq 2e^{-2kt^2} + e^{-k/6}.$$

Next, we can follow a similar argument in Wang (2022). Let  $\Delta = 1/\sqrt{k} + C(k/s)^{\alpha/d} = Cs^{-\alpha/(2\alpha+d)}$ ,  $A_0 = \{x : 0 < |\eta(x) - 1/2| < \Delta\}$  and  $A_j = \{x : 2^{j-1}\Delta < |\eta(x) - 1/2| < 2^j\Delta\}$  for  $j = 1, \dots, J := \lceil -\log(\Delta)/\log 2 \rceil$ . Write

$$\begin{aligned} r(\hat{h}_X) &= \mathbb{E}\left(|2\gamma(X) - 1| \mathbf{I}(\hat{h}_X(X) \neq h^*(X))\right) \\ &= \sum_{j=0}^J \mathbb{E}\left(|2\gamma(X) - 1| \mathbf{I}(\hat{h}_X(X) \neq h^*(X)) \mathbf{I}(X \in A_j)\right) \end{aligned}$$

We can work on each above term separately. Because  $\mathbf{I}(\hat{h}_X(X) \neq h^*(X)) \leq \mathbf{I}(|\gamma(X) - 1/2| < |\hat{\gamma}(X) - \gamma(X)|)$  and  $\beta$ -marginal assumption, so we can know

$$\begin{aligned}
& \mathbb{E} \left( |2\gamma(X) - 1| \mathbf{I}(\hat{h}_X(X) \neq h^*(X)) \mathbf{I}(X \in A_j) \right) \\
& \leq 2^{j+1} \Delta \mathbb{E} \left( \mathbf{I}(|\gamma(X) - 1/2| < |\hat{\gamma}(X) - \gamma(X)|) \mathbf{I}(X \in A_j) \right) \\
& \leq 2^{j+1} \Delta \mathbb{E} \left( \mathbf{I}(2^{j-1} \Delta < |\hat{\gamma}(X) - \gamma(X)|) \mathbf{I}(X \in A_j) \right) \\
& \leq 2^{j+1} \Delta \mathbb{E} \left( \mathbb{P}(2^{j-1} \Delta < |\hat{\gamma}(X) - \gamma(X)|) \mathbf{I}(X \in A_j) \right) \\
& \leq 2^{j+1} \Delta \mathbb{E} \left( (2e^{-2k(2^{j-1}\Delta)^2} + e^{-k/4}) \mathbf{I}(X \in A_j) \right) \\
& \leq 2^{j+1} \Delta 2e^{-2k(2^{j-1}\Delta)^2} (2^{j+1}\Delta)^\beta + e^{-k/4} 2^{j+1} \Delta \mathbb{P}(X \in A_j).
\end{aligned}$$

Putting these terms together, we can know that

$$r(\hat{h}_X) \leq C\Delta^{\beta+1} \leq C_S^{-\alpha(\beta+1)/(2\alpha+d)}.$$

## B.2.2 Proof for $\hat{h}_{\Theta_2(X)}$

Next, we work on  $\hat{h}_{\Theta_2(X)}$ . Recall the definition of  $\Theta_2(x)$  and define  $\tilde{\Theta}_2(\phi)$

$$\tilde{\Theta}_2(\phi) = (2l)^{(d+2)/4} \sqrt{2} (4\pi)^{d/4} (e^{-l\lambda_1} \eta_1(\phi), \dots, e^{-l\lambda_N} \eta_N(\phi)).$$

We also write  $\tilde{\Theta}_2(x) = \tilde{\Theta}_2(\phi)$  when  $x \in \mathcal{M}(\phi)$ . Since  $\tilde{\Theta}_2(x)$  is just scale version of  $\Theta_2(x)$ , it is sufficient to work on  $\hat{h}_{\tilde{\Theta}_2(X)}$ . If we choose  $l$  and  $N$  appropriately, the map  $\tilde{\Theta}_2(\phi)$  defined above is almost an isometry. Specifically, the Theorem 5.1 in Portegies (2016) suggests there exists  $l_0$  and  $N_0$  such that if we choose  $l = l_0$  and  $N > N_0$  in  $\tilde{\Theta}_2(\phi)$ , then  $\tilde{\Theta}_2(\phi)$  is an embedding of  $\mathcal{N}_s$  to  $\mathbb{R}^N$  and

$$\sup_{v \in T_\phi \mathcal{M}, \|v\|=1} \left| \left\| (D\tilde{\Theta}_2)_\phi(v) \right\|^2 - 1 \right| < \frac{1}{4}, \quad \forall \phi \in \mathcal{N}_s,$$

where  $(D\tilde{\Theta}_2)_\phi : T_\phi \mathcal{N}_s \rightarrow T_{\tilde{\Theta}_2(\phi)} \mathcal{N}'_s$  is the derivative of  $\tilde{\Theta}_2(\phi)$  at  $\phi$ . Here,  $\mathcal{N}'_s = \tilde{\Theta}_2(\mathcal{N}_s)$  is a manifold in  $\mathbb{R}^N$ . For any  $\phi_1, \phi_2 \in \mathcal{N}_s$  and a curve connecting  $\tilde{\Theta}_2(\phi_1)$  and  $\tilde{\Theta}_2(\phi_2)$ ,  $\chi : [0, 1] \rightarrow \mathcal{N}'_s$ , we can know that  $\tilde{\Theta}_2^{-1} \circ \chi$  is a curve in  $\mathcal{N}_s$ . Note that

$$d_{\mathcal{N}'_s}(\phi_1, \phi_2) \leq \int_0^1 \|D(\tilde{\Theta}_2^{-1} \circ \chi)(a)\| da \leq 2 \int_0^1 \|D\chi(a)\| da.$$

So we can conclude  $d_{\mathcal{N}_s}(\phi_1, \phi_2) \leq 2d_{\mathcal{N}'_s}(\tilde{\Theta}_2(\phi_1), \tilde{\Theta}_2(\phi_2))$  if taking the infimum of all possible curves  $\chi$ . Similarly, For any  $\phi_1, \phi_2 \in \mathcal{N}_s$  and a curve connecting  $\phi_1$  and  $\phi_2$ ,  $\chi : [0, 1] \rightarrow \mathcal{N}_s$ , we can know that  $\tilde{\Theta}_2 \circ \chi$  is a curve in  $\mathcal{N}'_s$ . Note that

$$d_{\mathcal{N}'_s}(\tilde{\Theta}_2(\phi_1), \tilde{\Theta}_2(\phi_2)) \leq \int_0^1 \left\| D(\tilde{\Theta}_2 \circ \chi)(a) \right\| da \leq 2 \int_0^1 \|D\chi(a)\| da.$$

So we know  $d_{\mathcal{N}'_s}(\tilde{\Theta}_2(\phi_1), \tilde{\Theta}_2(\phi_2)) \leq 2d_{\mathcal{N}_s}(\phi_1, \phi_2)$ . Therefore, we can conclude

$$\frac{1}{2}d_{\mathcal{N}_s}(\phi_1, \phi_2) \leq d_{\mathcal{N}'_s}(\tilde{\Theta}_2(\phi_1), \tilde{\Theta}_2(\phi_2)) \leq 2d_{\mathcal{N}_s}(\phi_1, \phi_2).$$

If we adopt  $\tilde{\Theta}_2(x)$ , the main difference in proof for convergence rate of  $k$ NN is the shape of neighborhood. Instead of  $\mathcal{B}(x, r, \|\cdot\|)$ , we consider the following small ball defined by  $\tilde{\Theta}_2(x)$

$$\mathcal{B}(x, r, \|\cdot\|_{\tilde{\Theta}_2}) = \{y \in \mathcal{M} : \|\tilde{\Theta}_2(x) - \tilde{\Theta}_2(y)\| \leq r\}.$$

Similarly, we can define  $r_a$  as the radius such that  $\mu(\mathcal{B}(x, r_a, \|\cdot\|_{\tilde{\Theta}_2})) = a$ . It is sufficient to characterize  $\sup_{y \in \mathcal{B}(x, r_{2k/s}, \|\cdot\|_{\tilde{\Theta}_2})} |\gamma(y) - \gamma(x)|$  as the rest of proof is the same with the case of  $\hat{h}_X$ . As  $\|\tilde{\Theta}_2(x) - \tilde{\Theta}_2(y)\| \leq d_{\mathcal{N}'_s}(\tilde{\Theta}_2(x), \tilde{\Theta}_2(y)) \leq 2d_{\mathcal{N}_s}(\phi_x, \phi_y)$  where  $x \in \mathcal{M}(\phi_x)$  and  $y \in \mathcal{M}(\phi_y)$ , we have

$$\mathcal{B}(x, r/2, d_{\mathcal{N}_s}) = \{y \in \mathcal{M} : d_{\mathcal{N}_s}(\phi_x, \phi_y) \leq r/2\} \subset \mathcal{B}(x, r, \|\cdot\|_{\tilde{\Theta}_2}).$$

We can apply the Bishop-Gromov inequality and the fact  $\mathcal{M} = T(\mathcal{N}_s \times \mathcal{N}_v)$  to have

$$\text{Vol}\mathcal{B}(x, r/2, d_{\mathcal{N}_s}) = \text{Vol}\mathcal{N}_v \times \text{Vol}\{\phi_y \in \mathcal{N}_s : d_{\mathcal{N}_s}(\phi_x, \phi_y) \leq r/2\} \geq \text{Vol}\mathcal{N}_v w_{d_s} (r/2)^{d_s},$$

which immediately leads to

$$f_{\min} \text{Vol}\mathcal{N}_v w_{d_s} r_{2k/s}^{d_s} / 2^{d_s} \leq \frac{2k}{s}.$$

Thus, we can conclude  $r_{2k/s} \leq C(2k/s)^{1/d_s}$ . If  $\|\tilde{\Theta}_2(x) - \tilde{\Theta}_2(y)\| \leq r_{2k/s}$ , then

$$d_{\mathcal{N}_s}(\phi_x, \phi_y) \leq 2d_{\mathcal{N}'_s}(\tilde{\Theta}_2(\phi_x), \tilde{\Theta}_2(\phi_y)) \leq 2r_{2k/s}(1 + Cr_{2k/s}) \leq C(2k/s)^{1/d_s}.$$

This leads to that if  $\|\tilde{\Theta}_2(x) - \tilde{\Theta}_2(y)\| \leq r_{2k/s}$ , then

$$|\gamma(y) - \gamma(x)| = |\tilde{\gamma}(\phi_y) - \tilde{\gamma}(\phi_x)| \leq Ld_{\mathcal{N}_s}(\phi_x, \phi_y)^\alpha \leq C(k/s)^{\alpha/d_s}.$$

An application of the same arguments in the proof for  $\hat{h}_X$  suggests

$$r(\hat{h}_{\Theta_2(X)}) \leq C \left( \frac{1}{\sqrt{k}} + C \left( \frac{k}{s} \right)^{\alpha/d_s} \right)^{\beta+1} \leq Cs^{-\alpha(\beta+1)/(2\alpha+d_s)}.$$

### B.2.3 Proof for $\hat{h}_{\Theta_1(X)}$

Finally, we work on  $\hat{h}_{\Theta_1(X)}$ . Note that

$$\|\tilde{\Theta}_2(x) - \tilde{\Theta}_2(y)\| \leq \|\tilde{\Theta}_1(x) - \tilde{\Theta}_1(y)\| \leq e^{l_0 \lambda_{N_0}} \|\tilde{\Theta}_2(x) - \tilde{\Theta}_2(y)\|.$$

We can apply the similar arguments to obtain

$$r(\hat{h}_{\Theta_1(X)}) \leq C \left( \frac{1}{\sqrt{k}} + C e^{\alpha l_0 \lambda_{N_0}} \left( \frac{k}{s} \right)^{\alpha/d_s} \right)^{\beta+1} \leq C (e^{-d_s l_0 \lambda_{N_0}} s)^{-\alpha(\beta+1)/(2\alpha+d_s)}.$$

## B.3 Proof for Theorem 3

### B.3.1 Proof for $\hat{h}_{\hat{\Theta}_2(X)}$

When we adopt a different data representation in  $k$ -NN, the main difference in the proof is the shape of neighborhood. Specifically, we need to consider the following neighborhood

$$\mathcal{B}(x, r, \|\cdot\|_{\hat{\Theta}_2}) = \{y \in \mathcal{M} : \|\hat{\Theta}_2(x) - \hat{\Theta}_2(y)\| \leq r\}.$$

We define  $r_a$  as the radius such that  $\mu(\mathcal{B}(x, r_a, \|\cdot\|_{\hat{\Theta}_2})) = a$ . By Proposition 1, we can know that

$$c\|\Theta_2(x) - \Theta_2(y)\| - c\sqrt{N_0}\epsilon_m \leq \|\hat{\Theta}_2(x) - \hat{\Theta}_2(y)\| \leq C\|\Theta_2(x) - \Theta_2(y)\| + C\sqrt{N_0}\epsilon_m$$

where  $\epsilon_m = (\log m/m)^{1/(4d+13)}$ . Therefore, we can know that

$$\mathcal{B}\left(x, \frac{r - C\sqrt{N_0}\epsilon_m}{C}, \|\cdot\|_{\Theta_2}\right) \subset \mathcal{B}(x, r, \|\cdot\|_{\hat{\Theta}_2})$$

Following the same arguments in the proof of Theorem 2, we have

$$r_{2k/s} - C\sqrt{N_0}\epsilon_m \leq C \left( \frac{k}{s} \right)^{1/d_s}.$$

Hence, we can conclude that when  $y \in \mathcal{B}(x, r_{2k/s}, \|\cdot\|_{\hat{\Theta}_2})$ ,

$$d_{\mathcal{N}_s}(\phi_x, \phi_y) \leq C \left( \frac{k}{s} \right)^{1/d_s} + C\sqrt{N_0}\epsilon_m,$$

where  $x \in \mathcal{M}(\phi_x)$  and  $y \in \mathcal{M}(\phi_y)$ . This immediately suggests

$$r(\hat{h}_{\hat{\Theta}_2(X)}) \leq C \left( \frac{1}{\sqrt{k}} + C \left( \frac{k}{s} \right)^{\alpha/d_s} + C\epsilon_m^\alpha \right)^{\beta+1} \leq C (s^{-\alpha(\beta+1)/(2\alpha+d_s)} + \epsilon_m^{\alpha(\beta+1)}).$$



### B.3.2 Proof for $\hat{h}_{\hat{\Theta}_1(X)}$

We can have the similar conclusion if we note that

$$c\|\Theta_1(x) - \Theta_1(y)\| - c\sqrt{N_0}\epsilon_m \leq \|\hat{\Theta}_1(x) - \hat{\Theta}_1(y)\| \leq C\|\Theta_1(x) - \Theta_1(y)\| + C\sqrt{N_0}\epsilon_m.$$

## B.4 Proof for Proposition 1

The main idea in the proof is to apply a similar strategy in Dunson et al. (2021), but we will point out the difference and provide the new gradients necessary for the new proof. See also Von Luxburg et al. (2008). The main difference is due to the facts that we use a randomized kernel and we do not normalize the eigenvectors. We divided the proof in five steps. Recall the definition

$$\tilde{h}_t^{(1)}(\phi_1, \phi_2) = \frac{\tilde{h}_t(\phi_1, \phi_2)}{f_{s,t}(\phi_1)f_{s,t}(\phi_2)}, \quad \text{where } f_{s,t}(\phi_1) = \int \tilde{h}_t(\phi_1, \phi_2)f_s(\phi_2)d\phi_2$$

and

$$\mathcal{P}_{t,1}g(\phi_1) = \int \frac{\tilde{h}_t^{(1)}(\phi_1, \phi_2)}{D_t^{(1)}(\phi_1)}g(\phi_2)f_s(\phi_2)d\phi_2, \quad \text{where } D_t^{(1)}(\phi_1) = \int \tilde{h}_t^{(1)}(\phi_1, \phi_2)f_s(\phi_2)d\phi_2.$$

Similarly, we define the corresponding empirical version

$$\tilde{h}_{m,t}^{(1)}(\phi, \phi') = \frac{\tilde{h}_t(\phi, \phi')}{f_{s,m,t}(\phi)f_{s,m,t}(\phi')}, \quad \text{where } f_{s,m,t}(\phi) = \frac{1}{m} \sum_{i=1}^m \tilde{h}_t(\phi, \phi_i)$$

and

$$\mathcal{P}_{m,t,1}g(\phi) = \frac{1}{m} \sum_{i=1}^m \frac{\tilde{h}_{m,t}^{(1)}(\phi, \phi_i)}{D_{m,t}^{(1)}(\phi)}g(\phi_i), \quad \text{where } D_{m,t}^{(1)}(\phi) = \frac{1}{m} \sum_{i=1}^m \tilde{h}_{m,t}^{(1)}(\phi, \phi_i).$$

The discrete version operator defined by  $\tilde{h}_t(\phi, \phi')$  can be written as

$$\tilde{W}^{(1)} = \tilde{D}^{-1}\tilde{W}\tilde{D}^{-1}, \quad \text{where } \tilde{D}_{i,i} = \frac{1}{m} \sum_j \tilde{W}_{i,j}$$

and

$$\tilde{P}^{(1)} = (\tilde{D}^{(1)})^{-1}\tilde{W}^{(1)}, \quad \text{where } \tilde{D}_{i,i}^{(1)} = \sum_j \tilde{W}_{i,j}^{(1)}$$

Different from  $P^{(1)}$ , the weight is defined as  $\tilde{W}_{i,j} = \tilde{h}_t(\phi_i, \phi_j)$  in  $\tilde{P}^{(1)}$ . Recall  $P^{(1)}$  can be written as the following equivalent form

$$W^{(1)} = D^{-1}WD^{-1}, \quad \text{where} \quad D_{i,i} = \frac{1}{m} \sum_j W_{i,j}$$

and

$$P^{(1)} = (D^{(1)})^{-1}W^{(1)}, \quad \text{where} \quad D_{i,i}^{(1)} = \sum_j W_{i,j}^{(1)}.$$

#### B.4.1 Step 1: spectral convergence of $(I - \mathcal{P}_{t,1})/t$ to $\mathcal{L}_{\mathcal{N}_s}$

To show the convergence, we define the heat kernel based operator  $\mathcal{H}_t$  on  $\mathcal{N}_s$

$$\mathcal{H}_t g(\phi_1) = \int H_t(\phi_1, \phi_2) g(\phi_2) d\phi_2, \quad \text{where} \quad H_t(\phi_1, \phi_2) = \sum_{l=0}^{\infty} e^{-\lambda_l t} \eta_l(\phi_1) \eta_l(\phi_2),$$

where  $\lambda_1, \dots$  and  $\eta(\phi), \dots$  are the eigenvalues and eigenvectors of  $\mathcal{L}_{\mathcal{N}_s}$ . Given  $\mathcal{H}_t$ , we can also define a residue operator  $\mathcal{R}_t = (I - \mathcal{H}_t)/t - (I - \mathcal{P}_{t,1})/t = (\mathcal{P}_{t,1} - \mathcal{H}_t)/t$ . Lemma 7 and 8 characterize the properties of  $\mathcal{R}_t$  in our setting. After introducing Lemma 6, 7, and 8, we can study the convergence of  $(I - \mathcal{P}_{t,1})/t$  in the same way as Dunson et al. (2021) (see its Proposition 1). Specifically, if we denote the eigenfunction and eigenvalue of  $(I - \mathcal{P}_{t,1})/t$  by  $(\lambda_{l,t}, \eta_{l,t})$  for  $l = 1, \dots, N$ , we can show that when  $t$  is smaller than some constant depending on  $\lambda_N$  and  $\Gamma_N$ , then

$$|\lambda_{l,t} - \lambda_l| \leq t^{3/4}, \quad \|a_l \eta_{l,t} - \eta_l\| \leq t^{3/4}, \quad \text{and} \quad \|a_l \eta_{l,t} - \eta_l\|_{\infty} \leq t^{1/2},$$

where  $a_l \in \{-1, 1\}$ .

#### B.4.2 Step 2: convergence of $\mathcal{P}_{m,t,1}$ to $\mathcal{P}_{t,1}$

To show the convergence of  $\mathcal{P}_{m,t,1}$ , we need to study the following the process

$$\sup_{\phi' \in \mathcal{N}_s} \left| \frac{1}{m} \sum_{i=1}^m \tilde{h}_t(\phi_i, \phi') - \int_{\mathcal{N}_s} \tilde{h}_t(\phi, \phi') f_s(\phi) d\phi \right|,$$

$$\sup_{\phi' \in \mathcal{N}_s} \left| \frac{1}{m} \sum_{i=1}^m g(\phi_i) \tilde{h}_t^{(1)}(\phi_i, \phi') - \int_{\mathcal{N}_s} g(\phi) \tilde{h}_t^{(1)}(\phi, \phi') f_s(\phi) d\phi \right|,$$

and

$$\sup_{\phi', \phi'' \in \mathcal{N}_s} \left| \frac{1}{m} \sum_{i=1}^m \tilde{h}_t^{(1)}(\phi_i, \phi'') \tilde{h}_t^{(1)}(\phi_i, \phi') - \int_{\mathcal{N}_s} \tilde{h}_t^{(1)}(\phi, \phi'') \tilde{h}_t^{(1)}(\phi, \phi') f_s(\phi) d\phi \right|.$$

The Lemma 5 help characterize the convergence of the above empirical process. After having Lemma 5, we can then apply the same arguments in Proposition 3 of Dunson et al. (2021) to show that if  $m$  is large enough so that  $(\sqrt{-\log t} + \sqrt{\log m}) / \sqrt{mt^{d/2}} < C$ , then

$$|\lambda_{l,t} - \lambda_{l,m,t}| \leq \frac{C}{\sqrt{mt^{(2d+5)/2}}} \left( \sqrt{-\log t} + \sqrt{\log m} \right)$$

and

$$\|a_l \eta_{l,t} - \eta_{l,m,t}\|_\infty \leq \frac{C}{\sqrt{mt^{(2d+3)/2}}} \left( \sqrt{-\log t} + \sqrt{\log m} \right)$$

with probability at least  $1 - m^{-2}$ . Here  $(\lambda_{l,m,t}, \eta_{l,m,t})$  for  $l = 1, \dots, N$  are the eigenvalues and eigenfunctions of  $(I - \mathcal{P}_{m,t,1})/t$ .

### B.4.3 Step 3: connection between $\mathcal{P}_{m,t,1}$ and $\tilde{P}^{(1)}$

This step aims to build the connection between  $\mathcal{P}_{m,t,1}$  and  $\tilde{P}^{(1)}$ , that is, there is a one-to-one correspondence between the eigenpairs of  $\mathcal{P}_{m,t,1}$  and the eigenpairs of  $\tilde{P}^{(1)}$ . Specifically, let  $(\lambda, g(\phi))$  be an eigenpair of  $\mathcal{P}_{m,t,1}$  and  $\vec{g}$  be a  $m$ -dimensional vector such that  $\vec{g}_i = g(\phi_i)$ . Note that

$$\begin{aligned} [\tilde{P}^{(1)} \vec{g}]_i &= \frac{\sum_{i'} \tilde{W}_{i,i'}^{(1)} g(\phi_{i'})}{\sum_{i'} \tilde{W}_{i,i'}^{(1)}} = \frac{\sum_{i'} \tilde{W}_{i,i'} g(\phi_{i'}) / \tilde{D}_{i,i} \tilde{D}_{i',i'}}{\sum_{i'} \tilde{W}_{i,i'} / \tilde{D}_{i,i} \tilde{D}_{i',i'}} \\ &= \frac{\sum_{i'} \tilde{h}_t(\phi_i, \phi_{i'}) g(\phi_{i'}) / f_{s,m,t}(\phi_i) f_{s,m,t}(\phi_{i'})}{\sum_{i'} \tilde{h}_t(\phi_i, \phi_{i'}) / f_{s,m,t}(\phi_i) f_{s,m,t}(\phi_{i'})} \\ &= \frac{\sum_{i'} \tilde{h}_{m,t}^{(1)}(\phi_i, \phi_{i'}) g(\phi_{i'})}{\sum_{i'} \tilde{h}_{m,t}^{(1)}(\phi_i, \phi_{i'})} \\ &= \mathcal{P}_{m,t,1} g(\phi_i) = \lambda g(\phi_i). \end{aligned}$$

Therefore,  $(\lambda, \vec{g})$  is an eigenpair of  $\tilde{P}^{(1)}$ .

On the other hand, let  $(\lambda, \vec{g})$  be an eigenpair of  $\tilde{P}^{(1)}$ . Given  $\vec{g}$ , define a function

$$g(\phi) = \frac{1}{\lambda} \frac{\sum_{i'} \tilde{h}_t(\phi, \phi_{i'}) \vec{g}_{i'} / f_{s,m,t}(\phi) f_{s,m,t}(\phi_{i'})}{\sum_{i'} \tilde{h}_t(\phi, \phi_{i'}) / f_{s,m,t}(\phi) f_{s,m,t}(\phi_{i'})}.$$

It is easy to check that

$$g(\phi_i) = \frac{1}{\lambda} \frac{\sum_{i'} \tilde{h}_t(\phi_i, \phi_{i'}) \vec{g}_{i'} / f_{s,m,t}(\phi_i) f_{s,m,t}(\phi_{i'})}{\sum_{i'} \tilde{h}_t(\phi_i, \phi_{i'}) / f_{s,m,t}(\phi_i) f_{s,m,t}(\phi_{i'})} = \frac{1}{\lambda} [\tilde{P}^{(1)} \vec{g}]_i = \vec{g}_i$$

and

$$\begin{aligned} \mathcal{P}_{m,t,1} g(\phi) &= \frac{\sum_{i'} \tilde{h}_t(\phi, \phi_{i'}) g(\phi_{i'}) / f_{s,m,t}(\phi) f_{s,m,t}(\phi_{i'})}{\sum_{i'} \tilde{h}_t(\phi, \phi_{i'}) / f_{s,m,t}(\phi) f_{s,m,t}(\phi_{i'})} \\ &= \frac{\sum_{i'} \tilde{h}_t(\phi, \phi_{i'}) \vec{g}_{i'} / f_{s,m,t}(\phi) f_{s,m,t}(\phi_{i'})}{\sum_{i'} \tilde{h}_t(\phi, \phi_{i'}) / f_{s,m,t}(\phi) f_{s,m,t}(\phi_{i'})} \\ &= \lambda g(\phi). \end{aligned}$$

Therefore,  $(\lambda, g(\phi))$  is an eigenpair of  $\mathcal{P}_{m,t,1}$ . So we prove that each eigenpair of  $\tilde{P}^{(1)}$  corresponds to each eigenpair of  $\mathcal{P}_{m,t,1}$ . For each eigenpair of  $(I - \mathcal{P}_{m,t,1})/t$ , i.e.,  $(\lambda_{l,m,t}, \eta_{l,m,t})$ , we write the corresponding eigenpair of  $(I - \tilde{P}^{(1)})/t$  as  $(\lambda_{l,m,t}, \vec{\eta}_{l,m,t})$ .

#### B.4.4 Step 4: convergence of $P^{(1)}$ to $\tilde{P}^{(1)}$

Similar to Step 2, the idea is to apply perturbation theory for spectral projections (see, e.g., Atkinson, 1967). Recall  $\vec{\eta}_{l,m,t}$  is the eigenvector of  $\tilde{P}^{(1)}$ . Let  $\vec{\eta}_{l,m,n,t}$  be the eigenvector of  $P^{(1)}$  and  $\text{Pr}_{\vec{\eta}_{l,m,n,t}}$  be the projection on  $\vec{\eta}_{l,m,n,t}$ . We can apply Theorem 3 in Atkinson (1967) or Theorem 5 in Dunson et al. (2021) to have

$$\|\vec{\eta}_{l,m,t} - \text{Pr}_{\vec{\eta}_{l,m,n,t}} \vec{\eta}_{l,m,t}\|_\infty \leq 8 \left( \left\| (P^{(1)} - \tilde{P}^{(1)}) \frac{\vec{\eta}_{l,m,t}}{\|\vec{\eta}_{l,m,t}\|_\infty} \right\|_\infty + \frac{48}{\Gamma_N t} \left\| (\tilde{P}^{(1)} - P^{(1)}) P^{(1)} \right\|_\infty \right) \|\vec{\eta}_{l,m,t}\|_\infty$$

An application of Lemma 1 and Lemma 2 suggests

$$\|\vec{\eta}_{l,m,t} - \text{Pr}_{\vec{\eta}_{l,m,n,t}} \vec{\eta}_{l,m,t}\|_\infty \leq \frac{1}{t} \left( \frac{C}{t^d \sqrt{mn}} \left( \sqrt{-\log t} + \sqrt{\log m} \right) + \frac{C t^{u-d/2} \sqrt{\log m}}{\sqrt{n}} \right) \|\vec{\eta}_{l,m,t}\|_\infty$$

with probability at least  $1 - m^{-2}$ . Following the same arguments in Proposition 3 of Dunson et al. (2021), we can show

$$|\lambda_{l,m,t} - \lambda_{l,m,n,t}| \leq \frac{C}{t^{(2d+5)/2} \sqrt{mn}} \left( \sqrt{-\log t} + \sqrt{\log m} \right) + \frac{C t^{u-(d+5)/2} \sqrt{\log m}}{\sqrt{n}}$$

and

$$\|a_l \vec{\eta}_{l,m,t} - \vec{\eta}_{l,m,n,t}\|_\infty \leq \frac{C}{t^{(2d+3)/2} \sqrt{mn}} \left( \sqrt{-\log t} + \sqrt{\log m} \right) + \frac{C t^{u-(d+3)/2} \sqrt{\log m}}{\sqrt{n}}$$

with probability at least  $1 - m^{-2}$ . Here,  $\lambda_{l,m,n,t}$  is the eigenvalue of  $(I - P^{(1)})/t$ .

### B.4.5 Step 5: finishing proof

We are ready to put the results from previous 4 steps together. Specifically, we have

$$|\lambda_l - \lambda_{l,m,n,t}| \leq t^{3/4} + \frac{C}{\sqrt{mt}^{(2d+5)/2}} \left( \sqrt{-\log t} + \sqrt{\log m} \right) + \frac{Ct^{u-(d+5)/2} \sqrt{\log m}}{\sqrt{n}}.$$

Since  $u > (d+5)/2 + 3/4$  and we choose  $t \asymp (\log m/m)^{2/(4d+13)}$ , we have

$$|\lambda_l - \lambda_{l,m,n,t}| \leq C \left( \frac{\log m}{m} \right)^{3/(8d+26)}.$$

To establish the bound for eigenvectors, we need to be aware of the difference in normalization for eigenfunctions and eigenvectors. The eigenfunction is normalized in the sense of  $L^2(\mathcal{N}_s)$ , while eigenvectors is normalized in the sense of  $\ell_2$  which relies on the density  $f_s(\phi)$ . Because  $1/\kappa < f_s(\phi) < \kappa$ , we can know that there exists a normalization constant  $c_{\kappa,l}$  such that  $1/\kappa < c_{\kappa,l} < \kappa$  and

$$|a_l c_{\kappa,l} [\vec{\eta}_{l,m,n,t}]_i - \eta_l(\phi_i)| \leq t^{1/2} + \frac{C}{\sqrt{mt}^{(2d+3)/2}} \left( \sqrt{-\log t} + \sqrt{\log m} \right) + \frac{Ct^{u-(d+3)/2} \sqrt{\log m}}{\sqrt{n}}.$$

Since  $u > (d+5)/2 + 3/4$  and we choose  $t \asymp (\log m/m)^{2/(4d+13)}$ , we have

$$|a_l c_{\kappa,l} [\vec{\eta}_{l,m,n,t}]_i - \eta_l(\phi_i)| \leq C \left( \frac{\log m}{m} \right)^{1/(4d+13)}.$$

We now complete the proof.

## B.5 Technical Lemmas and Proofs

**Lemma 1.** *Assume the assumptions in Lemma 3 hold. Then, we have*

$$\|(\tilde{P}^{(1)} - P^{(1)})P^{(1)}\|_\infty \leq \frac{C}{t^d \sqrt{mn}} \left( \sqrt{-\log t} + \sqrt{\log m} \right) + \frac{Ct^{u-d/2} \sqrt{\log m}}{\sqrt{n}}.$$

with probability at least  $1 - m^{-2}$ .

*Proof.* We introduce an intermediate operator between  $P^{(1)}$  and  $\tilde{P}^{(1)}$ , which is defined as

$$\bar{P}^{(1)} = (\tilde{D}^{(1)})^{-1} \bar{W}^{(1)}, \quad \text{where } \bar{W}^{(1)} = \tilde{D}^{-1} W \tilde{D}^{-1}.$$

By definition, we have

$$\begin{aligned}
\|(\tilde{P}^{(1)} - P^{(1)})P^{(1)}\|_\infty &\leq \|\tilde{P}^{(1)}P^{(1)} - \tilde{P}^{(1)}\bar{P}^{(1)}\|_\infty + \|\tilde{P}^{(1)}\bar{P}^{(1)} - \bar{P}^{(1)}\bar{P}^{(1)}\|_\infty \\
&\quad + \|\bar{P}^{(1)}\bar{P}^{(1)} - \bar{P}^{(1)}P^{(1)}\|_\infty + \|\bar{P}^{(1)}P^{(1)} - P^{(1)}P^{(1)}\|_\infty \\
&\leq \|P^{(1)} - \bar{P}^{(1)}\|_\infty (\|\tilde{P}^{(1)}\|_\infty + \|\bar{P}^{(1)}\|_\infty + \|P^{(1)}\|_\infty) + \|(\tilde{P}^{(1)} - \bar{P}^{(1)})\bar{P}^{(1)}\|_\infty \\
&\leq C\|P^{(1)} - \bar{P}^{(1)}\|_\infty + \|(\tilde{P}^{(1)} - \bar{P}^{(1)})\bar{P}^{(1)}\|_\infty.
\end{aligned}$$

Hence, it is sufficient to bound  $\|P^{(1)} - \bar{P}^{(1)}\|_\infty$  and  $\|(\tilde{P}^{(1)} - \bar{P}^{(1)})\bar{P}^{(1)}\|_\infty$ .

For  $\|P^{(1)} - \bar{P}^{(1)}\|_\infty$ , note that

$$\begin{aligned}
\|P^{(1)} - \bar{P}^{(1)}\|_\infty &= \sup_{g:|g_i|\leq 1} \sup_i |(P^{(1)} - \bar{P}^{(1)})g|_i \\
&= \sup_{g:|g_i|\leq 1} \sup_i \left| \frac{\sum_{i'} W_{i,i'}^{(1)} g_{i'}}{\sum_{i'} W_{i,i'}^{(1)}} - \frac{\sum_{i'} \bar{W}_{i,i'}^{(1)} g_{i'}}{\sum_{i'} \tilde{W}_{i,i'}^{(1)}} \right| \\
&\leq \sup_{g:|g_i|\leq 1} \sup_i \left( \left| \frac{\sum_{i'} W_{i,i'}^{(1)} g_{i'}}{\sum_{i'} W_{i,i'}^{(1)}} - \frac{\sum_{i'} W_{i,i'}^{(1)} g_{i'}}{\sum_{i'} \tilde{W}_{i,i'}^{(1)}} \right| + \left| \frac{\sum_{i'} W_{i,i'}^{(1)} g_{i'}}{\sum_{i'} \tilde{W}_{i,i'}^{(1)}} - \frac{\sum_{i'} \bar{W}_{i,i'}^{(1)} g_{i'}}{\sum_{i'} \tilde{W}_{i,i'}^{(1)}} \right| \right) \\
&\leq \sup_{g:|g_i|\leq 1} \sup_i \left( \left| \sum_{i'} W_{i,i'}^{(1)} g_{i'} \right| \frac{\left| \sum_{i'} W_{i,i'}^{(1)} - \sum_{i'} \tilde{W}_{i,i'}^{(1)} \right|}{\sum_{i'} W_{i,i'}^{(1)} \sum_{i'} \tilde{W}_{i,i'}^{(1)}} + \frac{\left| \sum_{i'} (W_{i,i'}^{(1)} - \bar{W}_{i,i'}^{(1)}) g_{i'} \right|}{\sum_{i'} \tilde{W}_{i,i'}^{(1)}} \right) \\
&\leq \sup_i \frac{\left| \sum_{i'} W_{i,i'}^{(1)} - \sum_{i'} \tilde{W}_{i,i'}^{(1)} \right|}{\sum_{i'} \tilde{W}_{i,i'}^{(1)}} + \sup_{g:|g_i|\leq 1} \sup_i \left( \frac{\left| \sum_{i'} (W_{i,i'}^{(1)} - \bar{W}_{i,i'}^{(1)}) g_{i'} \right|}{\sum_{i'} \tilde{W}_{i,i'}^{(1)}} \right) \\
&\leq \sup_i \frac{\left| \sum_{i'} W_{i,i'}^{(1)} - \sum_{i'} \tilde{W}_{i,i'}^{(1)} \right|}{\sum_{i'} \tilde{W}_{i,i'}^{(1)}} + \sup_{g:|g_i|\leq 1} \sup_i \left( \frac{1}{\sum_{i'} \tilde{W}_{i,i'}^{(1)}} \left| \sum_{i'} \left( \frac{W_{i,i'}}{D_{i,i} D_{i',i'}} - \frac{W_{i,i'}}{\tilde{D}_{i,i} \tilde{D}_{i',i'}} \right) g_{i'} \right| \right)
\end{aligned}$$

We can apply the similar arguments in the proof of Lemma 2 to show that

$$\|P^{(1)} - \bar{P}^{(1)}\|_\infty \leq \frac{C}{t^d \sqrt{mn}} \left( \sqrt{-\log t} + \sqrt{\log m} \right) + \frac{C t^{u-d/2} \sqrt{\log m}}{\sqrt{n}}.$$

For  $\|(\tilde{P}^{(1)} - \bar{P}^{(1)})\bar{P}^{(1)}\|_\infty$ , note that

$$\begin{aligned}
& \|(\tilde{P}^{(1)} - \bar{P}^{(1)})\bar{P}^{(1)}\|_\infty \\
&= \sup_{g:|g_i|\leq 1} \sup_i \left| [(\tilde{P}^{(1)} - \bar{P}^{(1)})\bar{P}^{(1)}g]_i \right| \\
&= \sup_i \sup_{g:|g_i|\leq 1} \left| \frac{1}{\sum_{i'} \tilde{W}_{i,i'}^{(1)}} \sum_{i'} \tilde{W}_{i,i'}^{(1)} \frac{\sum_{i''} \bar{W}_{i',i''}^{(1)} g_{i''}}{\sum_{i''} \tilde{W}_{i',i''}^{(1)}} - \frac{1}{\sum_{i'} \bar{W}_{i,i'}^{(1)}} \sum_{i'} \bar{W}_{i,i'}^{(1)} \frac{\sum_{i''} \bar{W}_{i',i''}^{(1)} g_{i''}}{\sum_{i''} \tilde{W}_{i',i''}^{(1)}} \right| \\
&\leq \sup_i \frac{1}{(\min_{i'} \sum_{i'} \tilde{W}_{i,i'}^{(1)})^2} \sup_{g:|g_i|\leq 1} \left( \min_{i'} \sum_{i'} \tilde{W}_{i,i'}^{(1)} \right) \left| \sum_{i'} \tilde{W}_{i,i'}^{(1)} \frac{\sum_{i''} \bar{W}_{i',i''}^{(1)} g_{i''}}{\sum_{i''} \tilde{W}_{i',i''}^{(1)}} - \sum_{i'} \bar{W}_{i,i'}^{(1)} \frac{\sum_{i''} \bar{W}_{i',i''}^{(1)} g_{i''}}{\sum_{i''} \tilde{W}_{i',i''}^{(1)}} \right| \\
&\leq \frac{1}{(\min_{i'} \sum_{i'} \tilde{W}_{i,i'}^{(1)})^2} \sup_i \sup_{g:|g_i|\leq 1} \left| \sum_{i'} \tilde{W}_{i,i'}^{(1)} \sum_{i''} \bar{W}_{i',i''}^{(1)} g_{i''} - \sum_{i'} \bar{W}_{i,i'}^{(1)} \sum_{i''} \bar{W}_{i',i''}^{(1)} g_{i''} \right| \\
&\leq Ct^d \sup_i \sup_{g:|g_i|\leq 1} \frac{\max_{i',i''} \bar{W}_{i',i''}^{(1)}}{m^2} \left| \sum_{i'} \tilde{W}_{i,i'}^{(1)} \sum_{i''} \frac{\bar{W}_{i',i''}^{(1)}}{\max_{i',i''} \bar{W}_{i',i''}^{(1)}} g_{i''} - \sum_{i'} \bar{W}_{i,i'}^{(1)} \sum_{i''} \frac{\bar{W}_{i',i''}^{(1)}}{\max_{i',i''} \bar{W}_{i',i''}^{(1)}} g_{i''} \right| \\
&\leq C \sup_i \sup_{g:|g_i|\leq 1} \left| \frac{1}{m} \sum_{i''} \left( \frac{1}{m} \sum_{i'} \tilde{W}_{i,i'}^{(1)} - \bar{W}_{i,i'}^{(1)} \right) g_{i''} \right|
\end{aligned}$$

By the definition, Lemma 4 and 3, we can show that

$$\begin{aligned}
\left| \frac{1}{m} \sum_{i'} \tilde{W}_{i,i'}^{(1)} - \bar{W}_{i,i'}^{(1)} \right| &= \frac{1}{\tilde{D}_{i,i} \tilde{D}_{i',i'}} \left| \frac{1}{m} \sum_{i'} (W_{i,i'} - \tilde{W}_{i,i'}) \right| \\
&\leq \frac{C}{t^d \sqrt{mn}} \left( \sqrt{-\log t} + \sqrt{\log m} \right) + \frac{Ct^{u-d/2} \sqrt{\log m}}{\sqrt{n}}.
\end{aligned}$$

Putting above terms together yields

$$\|(\tilde{P}^{(1)} - \bar{P}^{(1)})\bar{P}^{(1)}\|_\infty \leq \frac{C}{t^d \sqrt{mn}} \left( \sqrt{-\log t} + \sqrt{\log m} \right) + \frac{Ct^{u-d/2} \sqrt{\log m}}{\sqrt{n}}.$$

We now complete the proof.  $\square$

**Lemma 2.** *Assume the assumptions in Lemma 3 hold and let  $g = (g_1, \dots, g_m)$  be a  $m$ -dimensional vector such that  $|g_i| \leq 1$  for  $1 \leq i \leq m$ . Then, we have*

$$\|(\tilde{P}^{(1)} - P^{(1)})g\|_\infty \leq \frac{C}{t^d \sqrt{mn}} \left( \sqrt{-\log t} + \sqrt{\log m} \right) + \frac{Ct^{u-d/2} \sqrt{\log m}}{\sqrt{n}}.$$

with probability at least  $1 - m^{-2}$ .

*Proof.* By definition of  $P^{(1)}$  and  $\tilde{P}^{(1)}$ , we have

$$\begin{aligned}
\|(\tilde{P}^{(1)} - P^{(1)})g\|_\infty &= \sup_i \left| [(P^{(1)} - \tilde{P}^{(1)})g]_i \right| \\
&= \sup_i \left| \frac{\sum_{i'} W_{i,i'}^{(1)} g_{i'}}{\sum_{i'} W_{i,i'}^{(1)}} - \frac{\sum_{i'} \tilde{W}_{i,i'}^{(1)} g_{i'}}{\sum_{i'} \tilde{W}_{i,i'}^{(1)}} \right| \\
&\leq \sup_i \left| \frac{\sum_{i'} W_{i,i'}^{(1)} g_{i'}}{\sum_{i'} W_{i,i'}^{(1)}} - \frac{\sum_{i'} W_{i,i'}^{(1)} g_{i'}}{\sum_{i'} \tilde{W}_{i,i'}^{(1)}} \right| + \sup_i \left| \frac{\sum_{i'} W_{i,i'}^{(1)} g_{i'}}{\sum_{i'} \tilde{W}_{i,i'}^{(1)}} - \frac{\sum_{i'} \tilde{W}_{i,i'}^{(1)} g_{i'}}{\sum_{i'} \tilde{W}_{i,i'}^{(1)}} \right| \\
&\leq \sup_i \left| \sum_{i'} W_{i,i'}^{(1)} g_{i'} \right| \frac{\left| \sum_{i'} W_{i,i'}^{(1)} - \sum_{i'} \tilde{W}_{i,i'}^{(1)} \right|}{\sum_{i'} W_{i,i'}^{(1)} \sum_{i'} \tilde{W}_{i,i'}^{(1)}} + \sup_i \left| \frac{\sum_{i'} (W_{i,i'}^{(1)} - \tilde{W}_{i,i'}^{(1)}) g_{i'}}{\sum_{i'} \tilde{W}_{i,i'}^{(1)}} \right| \\
&\leq t^{d/2} \sup_i \left( \left| \frac{1}{m} \sum_{i'} (W_{i,i'}^{(1)} - \tilde{W}_{i,i'}^{(1)}) \right| + \left| \frac{1}{m} \sum_{i'} (W_{i,i'}^{(1)} - \tilde{W}_{i,i'}^{(1)}) g_{i'} \right| \right)
\end{aligned}$$

Hence, It is sufficient to bound the following terms

$$\left| \frac{1}{m} \sum_{i'} (W_{i,i'}^{(1)} - \tilde{W}_{i,i'}^{(1)}) g_{i'} \right| \quad \text{and} \quad \left| \frac{1}{m} \sum_{i'} (W_{i,i'}^{(1)} - \tilde{W}_{i,i'}^{(1)}) \right|.$$

Note that

$$\begin{aligned}
\left| \frac{1}{m} \sum_{i'} (W_{i,i'}^{(1)} - \tilde{W}_{i,i'}^{(1)}) g_{i'} \right| &= \left| \frac{1}{m} \sum_{i'} \left( \frac{W_{i,i'}}{D_{i,i} D_{i',i'}} - \frac{\tilde{W}_{i,i'}}{\tilde{D}_{i,i} \tilde{D}_{i',i'}} \right) g_{i'} \right| \\
&= \underbrace{\left| \frac{1}{m} \sum_{i'} \frac{(W_{i,i'} - \tilde{W}_{i,i'}) g_{i'}}{\tilde{D}_{i,i} \tilde{D}_{i',i'}} \right|}_{A_i} + \underbrace{\left| \frac{1}{m} \sum_{i'} \left( \frac{W_{i,i'}}{D_{i,i} D_{i',i'}} - \frac{W_{i,i'}}{\tilde{D}_{i,i} \tilde{D}_{i',i'}} \right) g_{i'} \right|}_{B_i}
\end{aligned}$$

We can bound  $A_i$  and  $B_i$  separately. For  $A_i$ , we can directly apply Lemma 4 and Lemma 3 to yield

$$A_i \leq \frac{C}{t^d \sqrt{mn}} \left( \sqrt{-\log t} + \sqrt{\log m} \right) + \frac{C t^{u-d/2} \sqrt{\log m}}{\sqrt{n}}.$$

For  $B_i$ , we have

$$\begin{aligned}
\left| \frac{W_{i,i'}}{D_{i,i} D_{i',i'}} - \frac{W_{i,i'}}{\tilde{D}_{i,i} \tilde{D}_{i',i'}} \right| &\leq \frac{|\tilde{D}_{i,i} \tilde{D}_{i',i'} - D_{i,i} D_{i',i'}|}{D_{i,i} D_{i',i'} \tilde{D}_{i,i} \tilde{D}_{i',i'}} \\
&\leq \frac{|\tilde{D}_{i',i'} - D_{i',i'}|}{D_{i,i} D_{i',i'} \tilde{D}_{i',i'}} + \frac{|\tilde{D}_{i,i} - D_{i,i}|}{D_{i,i} \tilde{D}_{i,i} \tilde{D}_{i',i'}} \\
&\leq \frac{C}{t^{3d/2} \sqrt{mn}} \left( \sqrt{-\log t} + \sqrt{\log m} \right) + \frac{C t^{u-d} \sqrt{\log m}}{\sqrt{n}}.
\end{aligned}$$



Here, we apply Lemma 4 and Lemma 3. This suggests

$$B_i \leq \frac{C}{t^{3d/2}\sqrt{mn}} \left( \sqrt{-\log t} + \sqrt{\log m} \right) + \frac{Ct^{u-d}\sqrt{\log m}}{\sqrt{n}}.$$

Putting all terms together, we have

$$\left| \frac{1}{m} \sum_{i'} (W_{i,i'}^{(1)} - \tilde{W}_{i,i'}^{(1)}) g_{i'} \right| \leq \frac{C}{t^{3d/2}\sqrt{mn}} \left( \sqrt{-\log t} + \sqrt{\log m} \right) + \frac{Ct^{u-d}\sqrt{\log m}}{\sqrt{n}}.$$

We can have a similar bound for  $\left| \sum_{i'} (W_{i,i'}^{(1)} - \tilde{W}_{i,i'}^{(1)})/m \right|$ . Then we can complete the proof.  $\square$

**Lemma 3.** *Suppose the assumptions in Lemma 4 hold and  $g = (g_1, \dots, g_m)$  is a  $m$ -dimensional vector such that  $|g_i| \leq 1$  for  $1 \leq i \leq m$ . If  $(\sqrt{-\log t} + \sqrt{\log m})/\sqrt{mt}^{d/2} < C$  and  $t^u\sqrt{\log m}/\sqrt{n} < C$ , with probability at least  $1 - m^{-2}$ , we have*

$$(a) \text{ For any } 1 \leq i \leq m, ct^{d/2} \leq \sum_{i'} W_{i,i'}/m \leq Ct^{d/2}$$

$$(b) \text{ For any } 1 \leq i \leq m, \left| \sum_{i'} W_{i,i'}^{(1)} g_{i'}/m \right| \leq Ct^{-d/2}$$

$$(c) \text{ For any } 1 \leq i \leq m, \sum_{i'} W_{i,i'}^{(1)}/m \geq ct^{-d/2}$$

$$(d) \|P^{(1)}\|_\infty \leq C \text{ and } \|\bar{P}^{(1)}\|_\infty \leq C$$

*Proof.* From Step 2 in proof of Proposition 1, we can know

$$ct^{d/2} \leq \frac{1}{m} \sum_{i'} \tilde{W}_{i,i'} \leq Ct^{d/2}.$$

By Lemma 4, we can know that

$$\left| \frac{1}{m} \sum_{i'} (W_{i,i'} - \tilde{W}_{i,i'}) \right| \leq \frac{C}{\sqrt{mn}} \left( \sqrt{-\log t} + \sqrt{\log m} \right) + \frac{Ct^{u+d/2}\sqrt{\log m}}{\sqrt{n}} \leq Ct^{d/2}.$$

So we can prove (a). For (b), note that

$$\left| \frac{1}{m} \sum_{i'} W_{i,i'}^{(1)} g_{i'} \right| = \left| \frac{1}{mD_{i,i}} \sum_{i'} \frac{W_{i,i'} g_{i'}}{D_{i',i'}} \right| \leq \frac{1}{(\min_i D_{i,i})^2} \left| \frac{1}{m} \sum_{i'} W_{i,i'} \right| \leq Ct^{-d/2}.$$

Similarly, for (c), we have

$$\frac{1}{m} \sum_{i'} W_{i,i'}^{(1)} = \frac{1}{mD_{i,i}} \sum_{i'} \frac{W_{i,i'}}{D_{i',i'}} \geq \frac{1}{(\max_i D_{i,i})^2} \frac{1}{m} \sum_{i'} W_{i,i'} \geq ct^{-d/2}.$$

After we have (b) and (c), we can naturally obtain (d).  $\square$

**Lemma 4.** Recall the definition of  $W_{i,i'}$  and  $\tilde{W}_{i,i'}$  in the proof of Proposition 1. Assume

$$\left| \frac{1}{\text{Vol}\mathcal{N}_v} \int_{\mathcal{M}(\phi_{i'})} \exp\left(-\frac{\|x-y\|^2}{t}\right) dx - \tilde{W}_{i,i'} \right| < C\tilde{W}_{i,i'}t^u, \quad y \in \mathcal{M}(\phi_i).$$

For any fixed  $g = (g_1, \dots, g_m)$  such that  $|g_i| \leq 1$ , we have

$$\mathbb{P}\left(\sup_{1 \leq i \leq m} \left| \frac{1}{m} \sum_{i'} (W_{i,i'} - \tilde{W}_{i,i'}) g_{i'} \right| \geq \frac{C}{\sqrt{mn}} \left( \sqrt{-\log t} + \sqrt{\log m} \right) + \frac{Ct^{u+d/2}\sqrt{\log m}}{\sqrt{n}} \right) \leq \frac{1}{m^2}.$$

*Proof.* We first decompose  $m^{-1} \sum_{i'} (W_{i,i'} - \tilde{W}_{i,i'}) g_{i'}$  into two parts

$$\begin{aligned} & \frac{1}{m} \sum_{i'} (W_{i,i'} - \tilde{W}_{i,i'}) g_{i'} \\ &= \underbrace{\frac{1}{m} \sum_{i'} (W_{i,i'} - \mathbb{E}(W_{i,i'} | \phi_{i'}, X_{i,1}, \dots, X_{i,n})) g_{i'}}_{A_i} + \underbrace{\frac{1}{m} \sum_{i'} (\mathbb{E}(W_{i,i'} | \phi_{i'}, X_{i,1}, \dots, X_{i,n}) - \tilde{W}_{i,i'}) g_{i'}}_{B_i}. \end{aligned}$$

We will bound the above terms  $A_i$  and  $B_i$  separately. To bound  $A_i$ , we define

$$U(Y) = \frac{1}{m} \sum_{i'} \left( \frac{1}{n} \sum_{j'=1}^n \exp\left(-\frac{\|Y - X_{i',j'}\|^2}{t}\right) - \frac{1}{\text{Vol}\mathcal{N}_v} \int_{\mathcal{M}(\phi_{i'})} \exp\left(-\frac{\|Y - x\|^2}{t}\right) dx \right) g_{i'},$$

where  $Y \in \mathcal{M}$ . Clearly,  $A_i = \sum_j U(X_{i,j})/n$ . We apply chaining technique (Talagrand, 2014; Wang et al., 2021) to establish a bound for  $\sup_{Y \in \mathcal{M}} |U(Y)|$ . For any fixed  $Y \in \mathcal{M}$ , an application of Hoeffding's inequality suggests

$$\mathbb{P}(|U(Y)| > r) \leq 2 \exp(-2mnr^2)$$

For any  $Y_1, Y_2 \in \mathcal{M}$ ,

$$\sup_x \left| \exp\left(-\frac{\|Y_1 - x\|^2}{t}\right) - \exp\left(-\frac{\|Y_2 - x\|^2}{t}\right) \right| \leq \frac{2\|Y_1 - Y_2\|}{t}.$$

We can apply Hoeffding's inequality again to yield

$$\mathbb{P}(|U(Y_1) - U(Y_2)| > r) \leq 2 \exp(-2mnt^2r^2/\|Y_1 - Y_2\|^2).$$

In addition, the same argument in the proof of Lemma 20 in Dunson et al. (2021) shows that

$$N(\mathcal{M}, \gamma, \|\cdot\|) \leq \left( \frac{8\text{diam}(\mathcal{M})}{\gamma} \right)^{d(3d+11)/2},$$

where  $N(\mathcal{M}, \gamma, \|\cdot\|)$  is the covering number of  $\mathcal{M}$  in the norm  $\|\cdot\|$ . Since  $\mathbb{E}(U(Y)) = 0$ , a standard chaining argument (see, e.g., Theorem 2.2.27 in Talagrand, 2014) suggests

$$\mathbb{P}\left(\sup_{Y \in \mathcal{M}} |U(Y)| > \frac{C}{\sqrt{mn}} \left(\sqrt{-\log t} + r\right)\right) \leq C \exp(-r^2).$$

Hence, we can know that

$$\mathbb{P}\left(|A_i| > \frac{C}{\sqrt{mn}} \left(\sqrt{-\log t} + \sqrt{\log m}\right)\right) \leq \frac{1}{2m^3}.$$

We then work on  $B_i$ . Given  $Y \in \mathcal{M}$ , define

$$V(Y) = \frac{1}{m} \sum_{i'=1}^m \left( \frac{1}{\text{Vol}\mathcal{N}_v} \int_{\mathcal{M}(\phi_{i'})} \exp\left(-\frac{\|x - Y\|^2}{t}\right) dx - \tilde{W}_{i,i'} \right) g_{i'}.$$

It is clear that  $B_i = \sum_{j=1}^n V(X_{i,j})/n$ . Since  $\mathbb{E}(V(X_{i,j})) = 0$

$$\left| \frac{1}{\text{Vol}\mathcal{N}_v} \int_{\mathcal{M}(\phi_{i'})} \exp\left(-\frac{\|x - Y\|^2}{t}\right) dx - \tilde{W}_{i,i'} \right| < C \tilde{W}_{i,i'} t^u,$$

an application of Hoeffding's inequality yields

$$\mathbb{P}(|B_i| > r) \leq 2 \exp\left(-\frac{2r^2}{nt^{2u}(\sum_{i'} \tilde{W}_{i,i'}/m)^2}\right).$$

Putting results of  $A_i$  and  $B_i$  together yields

$$\mathbb{P}\left(|A_i + B_i| > \frac{C}{\sqrt{mn}} \left(\sqrt{-\log t} + \sqrt{\log m}\right) + \frac{Ct^u \sqrt{\log m}}{\sqrt{n}} \left(\frac{1}{m} \sum_{i'} \tilde{W}_{i,i'}\right)\right) \leq \frac{1}{m^3}$$

We can complete the proof by applying union bound and noting  $\sum_{i'} \tilde{W}_{i,i'}/m \leq Ct^{d/2}$ .  $\square$

**Lemma 5.** *Let  $g(\phi)$  be a continuous function defined on  $\mathcal{N}_s$  such that  $\|g\|_\infty \leq 1$ . If  $t$  is a sufficiently small constant, then there is a constant  $C$  such that with probability at least  $1 - m^{-2}$ , we have*

$$\begin{aligned} & \sup_{\phi' \in \mathcal{N}_s} \left| \frac{1}{m} \sum_{i=1}^m \tilde{h}_t(\phi_i, \phi') - \int_{\mathcal{N}_s} \tilde{h}_t(\phi, \phi') f_s(\phi) d\phi \right| \leq \frac{C}{\sqrt{m}} \left(\sqrt{-\log t} + \sqrt{\log m}\right), \\ & \sup_{\phi' \in \mathcal{N}_s} \left| \frac{1}{m} \sum_{i=1}^m g(\phi_i) \tilde{h}_t^{(1)}(\phi_i, \phi') - \int_{\mathcal{N}_s} g(\phi) \tilde{h}_t^{(1)}(\phi, \phi') f_s(\phi) d\phi \right| \leq \frac{C}{\sqrt{mt^d}} \left(\sqrt{-\log t} + \sqrt{\log m}\right), \\ & \sup_{\phi', \phi'' \in \mathcal{N}_s} \left| \frac{1}{m} \sum_{i=1}^m \tilde{h}_t^{(1)}(\phi_i, \phi'') \tilde{h}_t^{(1)}(\phi_i, \phi') - \int_{\mathcal{N}_s} \tilde{h}_t^{(1)}(\phi, \phi'') \tilde{h}_t^{(1)}(\phi, \phi') f_s(\phi) d\phi \right| \\ & \leq \frac{C}{\sqrt{mt^{2d}}} \left(\sqrt{-\log t} + \sqrt{\log m}\right). \end{aligned}$$

*Proof.* If we can characterize the covering number of  $\mathcal{F}_1 = \{\tilde{h}_t(\cdot, \phi') : \phi' \in \mathcal{N}_s\}$ ,  $\mathcal{F}_2 = \{t^d g(\cdot) \tilde{h}_t(\cdot, \phi') : \phi' \in \mathcal{N}_s\}$ , and  $\mathcal{F}_3 = \{t^{2d} \tilde{h}_t(\cdot, \phi') \tilde{h}_t(\cdot, \phi'') : \phi', \phi'' \in \mathcal{N}_s\}$  in the norm  $\|\cdot\|_\infty$ , we can follow the same strategy in Proposition 2 in Dunson et al. (2021) to show the above statements. The rest of proof is to bound the covering number of  $\mathcal{F}_1$ ,  $\mathcal{F}_2$ , and  $\mathcal{F}_3$ . Recall the covering number of  $\mathcal{F}$ ,  $N(\mathcal{F}, \gamma, \|\cdot\|_\infty)$ , is defined as the smallest number of balls with radius  $\gamma$  in the norm  $\|\cdot\|_\infty$  that can cover  $\mathcal{F}$ . Following the same argument in the proof of Lemma 20 in Dunson et al. (2021), we can show that

$$N(\mathcal{N}_s, \gamma, d_{\mathcal{N}_s}(\cdot, \cdot)) \leq \left( \frac{8 \text{diam}(\mathcal{N}_s)}{\gamma} \right)^{d_s(3d_s+11)/2}.$$

Note that

$$\begin{aligned} & \max_{\phi \in \mathcal{N}_s} \left| \tilde{h}_t(\phi, \phi') - \tilde{h}_t(\phi, \phi'') \right| \\ &= \frac{1}{\text{Vol}^2 \mathcal{N}_v} \max_{\phi \in \mathcal{N}_s} \left| \int_{\mathcal{M}(\phi)} \int_{\mathcal{M}(\phi')} \exp\left(\frac{\|x-y\|^2}{t}\right) dx dy - \int_{\mathcal{M}(\phi)} \int_{\mathcal{M}(\phi'')} \exp\left(\frac{\|x-y\|^2}{t}\right) dx dy \right| \\ &= \frac{1}{\text{Vol}^2 \mathcal{N}_v} \max_{\phi \in \mathcal{N}_s} \left| \int_{\mathcal{M}(\phi)} \int_{\mathcal{N}_v} \exp\left(\frac{\|T(\phi', \psi) - y\|^2}{t}\right) - \exp\left(\frac{\|T(\phi'', \psi) - y\|^2}{t}\right) d\psi dy \right| \\ &\leq \frac{1}{\text{Vol}^2 \mathcal{N}_v} \max_{\phi \in \mathcal{N}_s} \int_{\mathcal{M}(\phi)} \int_{\mathcal{N}_v} \frac{d_{\mathcal{N}_s}(\phi', \phi'')}{2t} d\psi dy \\ &\leq \frac{d_{\mathcal{N}_s}(\phi', \phi'')}{2t} \end{aligned}$$

Here we use the mean value theorem. Therefore, we can know that

$$N(\mathcal{F}_1, \gamma, \|\cdot\|_\infty) \leq \left( \frac{4 \text{diam}(\mathcal{N}_s)}{t\gamma} \right)^{d_s(3d_s+11)/2}.$$

When  $\|g\|_\infty \leq 1$ , we have

$$\begin{aligned} & \max_{\phi \in \mathcal{N}_s} \left| g(\phi) \tilde{h}_t^{(1)}(\phi, \phi') - g(\phi) \tilde{h}_t^{(1)}(\phi, \phi'') \right| \\ &= \max_{\phi \in \mathcal{N}_s} \left| g(\phi) \frac{\tilde{h}_t(\phi, \phi')}{f_{s,t}(\phi) f_{s,t}(\phi')} - g(\phi) \frac{\tilde{h}_t(\phi, \phi'')}{f_{s,t}(\phi) f_{s,t}(\phi'')} \right| \\ &= \max_{\phi \in \mathcal{N}_s} \left| \frac{g(\phi)}{f_{s,t}(\phi)} \right| \left| \frac{\tilde{h}_t(\phi, \phi') f_{s,t}(\phi'') - \tilde{h}_t(\phi, \phi'') f_{s,t}(\phi')}{f_{s,t}(\phi') f_{s,t}(\phi'')} \right| \\ &= \max_{\phi \in \mathcal{N}_s} \left| \frac{g(\phi)}{f_{s,t}(\phi)} \right| \left| \frac{\tilde{h}_t(\phi, \phi') f_{s,t}(\phi'') - \tilde{h}_t(\phi, \phi'') f_{s,t}(\phi'') + \tilde{h}_t(\phi, \phi'') f_{s,t}(\phi'') - \tilde{h}_t(\phi, \phi'') f_{s,t}(\phi')}{f_{s,t}(\phi') f_{s,t}(\phi'')} \right| \\ &\leq \max_{\phi \in \mathcal{N}_s} \left| \frac{g(\phi)}{f_{s,t}(\phi)} \right| \left( \left| \frac{\tilde{h}_t(\phi, \phi') - \tilde{h}_t(\phi, \phi'')}{f_{s,t}(\phi')} \right| + \left| \frac{\tilde{h}_t(\phi, \phi'') (f_{s,t}(\phi'') - f_{s,t}(\phi'))}{f_{s,t}(\phi') f_{s,t}(\phi'')} \right| \right). \end{aligned}$$

The Lemma 6 (a) suggests there are constants  $C_1$  and  $C_2$  such that  $C_1 t^{d/2} \leq f_{s,t}(\phi) \leq C_2 t^{d/2}$ .

In addition, we have

$$|f_{s,t}(\phi'') - f_{s,t}(\phi')| = \left| \int \tilde{h}_t(\phi', \phi) f_s(\phi) d\phi - \int \tilde{h}_t(\phi'', \phi) f_s(\phi) d\phi \right| \leq \max_{\phi \in \mathcal{N}_s} \left| \tilde{h}_t(\phi, \phi') - \tilde{h}_t(\phi, \phi'') \right|.$$

Putting above together yields

$$\max_{\phi \in \mathcal{N}_s} \left| g(\phi) \tilde{h}_t^{(1)}(\phi, \phi') - g(\phi) \tilde{h}_t^{(1)}(\phi, \phi'') \right| \leq \frac{C}{t^{3d/2}} \max_{\phi \in \mathcal{N}_s} \left| \tilde{h}_t(\phi, \phi') - \tilde{h}_t(\phi, \phi'') \right| \leq \frac{C d_{\mathcal{N}_s}(\phi', \phi'')}{t^{(3d+2)/2}}.$$

So we have

$$N(\mathcal{F}_2, \gamma, \|\cdot\|_\infty) \leq \left( \frac{C \text{diam}(\mathcal{N}_s)}{t^{(d+2)/2} \gamma} \right)^{d_s(3d_s+11)/2}.$$

Similarly, we can show

$$N(\mathcal{F}_3, \gamma, \|\cdot\|_\infty) \leq \left( \frac{C \text{diam}(\mathcal{N}_s)}{t^{(d+2)/2} \gamma} \right)^{d_s(3d_s+11)/2}.$$

We now complete the proof. □

**Lemma 6.** *If we adopt the same notation in Lemma 9, then we have*

(a)  $f_{s,t}(\phi) = m_0 f_s(\phi) t^{d/2} + O(t^{(d+2)/2})$  and  $\tilde{h}_t^{(1)}(\phi_1, \phi_2) = (1 + O(t)) \tilde{h}_t(\phi_1, \phi_2) / m_0^2 f_s(\phi_1) f_s(\phi_2) t^d$ .

(b)  $\mathcal{P}_{t,1}$  is a self-adjoint operator.

(c) For any function  $g(\phi)$ ,  $\mathcal{P}_{t,1}g(\phi)$  is smooth function on  $\mathcal{N}_s$  and

$$\mathcal{P}_{t,1}g(\phi_1) = \frac{\int \tilde{h}_t(\phi_1, \phi_2) g(\phi_2) d\phi_2}{\int \tilde{h}_t(\phi_1, \phi_2) d\phi_2} + O(t).$$

(d) For any function  $g(\phi)$ ,

$$\frac{g(\phi) - \mathcal{P}_{t,1}g(\phi)}{t} = \mathcal{L}_{\mathcal{N}_s}g(\phi) + O(t).$$

*Proof.* We omit the proof here since we can apply the same arguments in Coifman and Lafon (2006) when we have Lemma 9. □

**Lemma 7.** *Let  $\mathcal{R}_t$  be the operator defined in proof for Proposition 1. For any function  $g(\phi)$ , there exists a constant  $C$  such that when  $t$  is small enough, then  $\|\mathcal{R}_t g\| \leq C \|g\|$ .*

*Proof.* Recall  $\mathcal{R}_t = (\mathcal{P}_{t,1} - \mathcal{H}_t)/t$ . By Lemma 6 (c), we have

$$\mathcal{P}_{t,1}g(\phi_1) = \frac{\int \tilde{h}_t(\phi_1, \phi_2)g(\phi_2)d\phi_2}{\int \tilde{h}_t(\phi_1, \phi_2)d\phi_2} + O(t).$$

The  $O(t)$  comes from the residue term in Lemma 9. If we dig into the proof details in Lemma 9, we can find that  $O(t^2)$  can also be written as  $O(t^2g(\phi))$ . Therefore, if we apply Lemma 9, we can have

$$\|\mathcal{P}_{t,1}g(\phi) - (g - t\mathcal{L}_{\mathcal{N}_s}(g))\| \leq O(t^2\|g\|).$$

By Lemma 3 (a) in Dunson et al. (2021), we can have

$$\left\| \mathcal{H}_t g(\phi) - \int (4\pi t)^{-d_s/2} e^{-\frac{d_{\mathcal{N}_s}(\phi, \phi')^2}{4t}} g(\phi') d\phi' \right\| \leq O(t\|g\|)$$

By the similar arguments in Lemma 9, we can know

$$\int (4\pi t)^{-d_s/2} e^{-\frac{d_{\mathcal{N}_s}(\phi, \phi')^2}{4t}} g(\phi') d\phi' = g - t\mathcal{L}_{\mathcal{N}_s}(g) + O(t^2g(\phi)).$$

Putting all above terms together leads to

$$\|\mathcal{R}_t g\| \leq (C + O(t))\|g\|.$$

□

**Lemma 8.** *Let  $\eta_l$  be the  $l$ th eigenfunction of  $\mathcal{L}_{\mathcal{N}_s}$  such that  $\|\eta_l\| = 1$ . There exists a constant  $C$  such that when  $t$  is small enough,  $\|\mathcal{R}_t \eta_l\| \leq Ct(1 + \lambda_l^{d_s/2+5})$ .*

*Proof.* Recall  $\mathcal{R}_t = (\mathcal{P}_{t,1} - \mathcal{H}_t)/t$ . By Lemma 6 (d), we have

$$\mathcal{P}_{t,1}\eta_l = \eta_l - t\lambda_l\eta_l + O(t^2)\eta_l.$$

By the definition of heat kernel, we have

$$\mathcal{H}_t\eta_l = e^{-\lambda_l t}\eta_l.$$

Therefore, we have

$$\|\mathcal{R}_t \eta_l\| \leq \frac{(1 - t\lambda_l - e^{-\lambda_l t})}{t} \eta_l + O(t)\eta_l \leq Ct(1 + \lambda_l^2).$$

We can apply a similar strategy in Lemma 8 of Dunson et al. (2021) to show

$$\|\mathcal{R}_t\eta\| \leq Ct(1 + \lambda_i^{d_s/2+5}).$$

□

**Lemma 9.** *If we write*

$$m_0 = \int_{\mathbb{R}^d} \exp(\|u\|^2) du \quad \text{and} \quad m_2 = \int_{\mathbb{R}^d} u_1^2 \exp(\|u\|^2) du,$$

then we have

$$G_t g(\phi) = m_0 g(\phi) - t \frac{m_2}{2} \mathcal{L}_{\mathcal{N}_s} g(\phi) + O(t^2).$$

*Proof.* We can rewrite  $G_t g(\phi)$  as

$$\begin{aligned} G_t g(\phi) &= \frac{1}{t^{d/2} \text{Vol}^2 \mathcal{N}_v} \int_{\mathcal{N}_s} \int_{\mathcal{M}(\phi)} \int_{\mathcal{M}(\phi')} \exp\left(-\frac{\|x-y\|^2}{t}\right) g(\phi') dx dy d\phi' \\ &= \frac{1}{t^{d/2} \text{Vol} \mathcal{N}_v} \int_{\mathcal{M}(\phi)} \int_{\mathcal{M}} \exp\left(-\frac{\|x-y\|^2}{t}\right) \left( \int_{\mathcal{N}_s} \mathbf{I}(y \in \mathcal{M}(\phi')) g(\phi') d\phi' \right) dy dx. \end{aligned}$$

If we define

$$\tilde{g}(y) = \int_{\mathcal{N}_s} \mathbf{I}(y \in \mathcal{M}(\phi')) g(\phi') d\phi',$$

then

$$G_t g(\phi) = \frac{1}{t^{d/2} \text{Vol} \mathcal{N}_v} \int_{\mathcal{M}(\phi)} \int_{\mathcal{M}} \exp\left(-\frac{\|x-y\|^2}{t}\right) \tilde{g}(y) dy dx.$$

Different from  $g(\phi)$ ,  $\tilde{g}(x)$  is defined on  $\mathcal{M}$ . It is clear that  $\tilde{g}(x) = \tilde{g}(y) = g(\phi)$  if  $x, y \in \mathcal{M}(\phi)$ .

To evaluate  $G_t g(\phi)$ , it is sufficient to work on

$$F_t \tilde{g}(x) = \frac{1}{t^{d/2}} \int_{\mathcal{M}} \exp\left(-\frac{\|x-y\|^2}{t}\right) \tilde{g}(y) dy.$$

We can first reduce the integral on a small ball  $\{y : \|x-y\| \leq r\}$  such that the exponential map is diffeomorphism within this small ball. Outside of the ball,

$$\frac{1}{t^{d/2}} \int_{y \in \mathcal{M}: \|x-y\| > r} \exp\left(-\frac{\|x-y\|^2}{t}\right) \tilde{g}(y) dy \leq C \sup_{y \in \mathcal{M}} |\tilde{g}(y)| \exp(-r^2/t) = O(t^2).$$

Hence, we have

$$F_t \tilde{g}(x) = \frac{1}{t^{d/2}} \int_{y \in \mathcal{M}: \|x-y\| \leq r} \exp\left(-\frac{\|x-y\|^2}{t}\right) \tilde{g}(y) dy + O(t^2).$$

At  $x \in \mathcal{M}$ , we write  $T_x\mathcal{M}$  as the tangent space of  $\mathcal{M}$  at  $x$ . Since  $\mathcal{M} = T(\mathcal{N}_s \times \mathcal{N}_v)$ , we can decompose the tangent space into two subspaces  $T_x\mathcal{M} = V_x\mathcal{M} \oplus H_x\mathcal{M}$ , where  $V_x\mathcal{M}$  is vertical space (corresponds to  $\mathcal{N}_v$ ) and  $H_x\mathcal{M}$  is horizontal space (corresponds to  $\mathcal{N}_s$ ). Let  $e_1, \dots, e_{d_s}, e_{d_s+1}, \dots, e_d$  be a fixed orthonormal basis of  $T_x\mathcal{M}$  such that  $e_1, \dots, e_{d_s}$  corresponds to the directions of  $\mathcal{N}_s$  and  $e_{d_s+1}, \dots, e_d$  corresponds to the directions of  $\mathcal{N}_v$ . By the exponential map  $\exp_x(s)$ , any point  $y$  in a small neighborhood of  $x$  has a set of normal coordinates  $s = (s_1, \dots, s_d)$ . Then, the function  $\tilde{g}(y)$  can be written as  $\tilde{g}^*(s_1, \dots, s_{d_s})$  since  $\tilde{g}(x) = \tilde{g}(y) = g(\phi)$  if  $x, y \in \mathcal{M}(\phi)$ . We can change variable as in Belkin and Niyogi (2008),

$$F_t \tilde{g}(x) = \frac{1}{t^{d/2}} \int_{\tilde{B}} \exp\left(-\frac{\|x - \exp_x(s)\|^2}{t}\right) \tilde{g}^*(s) (1 + O(\|s\|^2)) ds + O(t^2),$$

where  $\tilde{B}$  is the preimage of exponential map for  $\{y \in \mathcal{M} : \|x - y\| \leq r\}$ . By Lemma 4.3 in Belkin and Niyogi (2008), we have

$$0 \leq \|s\|^2 - \|\exp_x(s) - x\|^2 = w(s) \leq C\|s\|^4.$$

and

$$\exp\left(-\frac{\|\exp_x(s) - x\|^2}{t}\right) = \exp\left(-\frac{\|s\|^2 - w(s)}{t}\right) = \exp\left(-\frac{\|s\|^2}{t}\right) \left(1 + O\left(\frac{w(s)}{t} e^{w(s)/t}\right)\right).$$

Therefore, we have

$$\begin{aligned} F_t \tilde{g}(x) &= \frac{1}{t^{d/2}} \int_{\tilde{B}} \exp\left(-\frac{\|s\|^2}{t}\right) \left(1 + O\left(\frac{w(s)}{t} e^{w(s)/t}\right)\right) \tilde{g}^*(s) (1 + O(\|s\|^2)) ds + O(t^2) \\ &= A_t + B_t + C_t + O(t^2), \end{aligned}$$

where

$$\begin{aligned} A_t &= \frac{1}{t^{d/2}} \int_{\tilde{B}} \exp\left(-\frac{\|s\|^2}{t}\right) \tilde{g}^*(s) ds, \\ B_t &= \frac{1}{t^{d/2}} \int_{\tilde{B}} \exp\left(-\frac{\|s\|^2}{t}\right) \tilde{g}^*(s) O(\|s\|^2) ds, \end{aligned}$$

and

$$C_t = \frac{1}{t^{d/2}} \int_{\tilde{B}} \exp\left(-\frac{\|s\|^2}{t}\right) O\left(\frac{w(s)}{t} e^{w(s)/t}\right) \tilde{g}^*(s) (1 + O(\|s\|^2)) ds.$$

We can apply the similar arguments in Belkin and Niyogi (2008) to show that  $B_t = O(t^2)$  and  $C_t = O(t^2)$ . We now work on  $A_t$ . The Taylor expansion for  $\tilde{g}^*$  suggests

$$\tilde{g}^*(s_1, \dots, s_{d_s}) = \tilde{g}^*(0) + \sum_{k=1}^{d_s} s_k \frac{\partial \tilde{g}^*}{\partial s_k}(0) + \frac{1}{2} \sum_{k_1=1}^{d_s} \sum_{k_2=1}^{d_s} s_{k_1} s_{k_2} \frac{\partial^2 \tilde{g}^*}{\partial s_{k_1} \partial s_{k_2}}(0) + O(\|s\|^3).$$



Therefore, we have

$$\begin{aligned}
A_t &= \frac{1}{t^{d/2}} \int_{\tilde{B}} \exp\left(-\frac{\|s\|^2}{t}\right) \tilde{g}^*(0) ds + \sum_{k=1}^{d_s} \frac{1}{t^{d/2}} \int_{\tilde{B}} \exp\left(-\frac{\|s\|^2}{t}\right) s_k \frac{\partial \tilde{g}^*}{\partial s_k}(0) ds \\
&\quad + \frac{1}{2} \sum_{k_1=1}^{d_s} \sum_{k_2=1}^{d_s} \frac{1}{t^{d/2}} \int_{\tilde{B}} \exp\left(-\frac{\|s\|^2}{t}\right) s_{k_1} s_{k_2} \frac{\partial^2 \tilde{g}^*}{\partial s_{k_1} \partial s_{k_2}}(0) ds + \frac{1}{t^{d/2}} \int_{\tilde{B}} \exp\left(-\frac{\|s\|^2}{t}\right) O(\|s\|^3) ds \\
&= m_0 \tilde{g}^*(0) + \frac{t}{2} m_2 \sum_{k=1}^{d_s} \frac{\partial^2 \tilde{g}^*}{\partial s_k^2}(0) + O(t^2)
\end{aligned}$$

Putting  $A_t$ ,  $B_t$ , and  $C_t$  together leads to

$$F_t \tilde{g}(x) = m_0 \tilde{g}^*(0) + \frac{t}{2} m_2 \sum_{k=1}^{d_s} \frac{\partial^2 \tilde{g}^*}{\partial s_k^2}(0) + O(t^2).$$

Since  $\tilde{g}^*(s) = \tilde{g}(y) = g(\phi_y)$  and  $\mathcal{M} = T(\mathcal{N}_s \times \mathcal{N}_v)$ , we can know that

$$\sum_{k=1}^{d_s} \frac{\partial^2 \tilde{g}^*}{\partial s_k^2}(0) = -\mathcal{L}_{\mathcal{N}_s} g(\phi_x) \quad \text{and} \quad \tilde{g}^*(0) = g(\phi_x),$$

where  $x \in \mathcal{M}(\phi_x)$ . Plugging back to  $G_t g(\phi)$  yields

$$G_t g(\phi) = m_0 g(\phi) - \frac{t}{2} m_2 \mathcal{L}_{\mathcal{N}_s} g(\phi) + O(t^2).$$

□